Abstracts of Doctor's Thesises

Effect of "Topotactic" Reduction Products on Catalytic Activity of Metallocene Catalyst for Olefin Polymerization

Satoru Yamada †
(Department of Chemistry for Materials)

Keywords: Topotactic reduction, Tungsten disulfide, Molybdenum disulfide, Cocatalyst, Metallocene catalyst

1. Introduction

Metallocene catalysts, which consist of metallocene compounds and cocatalysts such as methylaluminoxane (MAO) or tetrakis(pentafluorophenyl)borate ($B(C_6F_5)_4^-$)-based salt, catalyze α-olefin polymerization to produce polymers with a narrow molecular weight distribution and a narrow composition distribution.

The catalytically active species in the polymerization have been confirmed to be cationic metallocene complexes with non-coordinating anions. The cocatalysts have been shown to convert neutral dialkylmetallocene (Cp_2MR_2) into the cationic monoalkylmetallocene (Cp_2MR^+) by way of protolysis or alkyl abstraction and provide the cationic species with the non-coordinating anions [eq. (1)].

$$Cp_2MR_2 + [R_3NH^+][B(C_6F_5)_4^-] \rightarrow [Cp_2MR^+][B(C_6F_5)_4^-] + RH + R_3N \quad (1)$$

Recently, we found that the salt of ammonium ion and anion obtained by "topotactic" reduction is a significantly effective cocatalyst in metallocene catalyst for the ethylene polymerization [1]. The "topotactic" reduction can be defined as the bulk reaction of an electronically conducting host lattice (Z) with vacant lattice sites (□) with electrons [eq. (2)].

$$xA^+ + xe^- + \square_x[Z] \rightarrow (A^+)_x[Z]^{x-} \quad (2)$$

The electrons are provided by concurrent chemical or electrochemical reactions and they enter into the conduction band of the host lattice. At the same time with the uptake of the electrons, an equivalent amount of mobile guest cation (A^+) of electrolyte might diffuse from the host/electrolyte interface to the vacant lattice site of the host lattice. Therefore, basic structural integrity of the host matrix is retained during the course of the reaction (topotactic process). The solid in the reduced state is shown as a macroanion matrix $[Z]^{x-}$ with intercalated mobile guest cation A^+. Here, on the basis of the structural characteristics, the host lattice (Z) may be divided into the following three kinds of categories: three-dimensional system, two-dimensional system, and one-dimensional system. To investigate the effect of "topotactic" reduction product on the catalytic activity of metallocene catalyst for olefin polymerization, we selected the two-dimensional systems as a host lattice with the accommodation for alkyl ammonium ion such as *N*,*N*-Dimethylanilinium ion ($Ph(Me)_2NH^+$) that was one of cations capable of effectively converting Cp_2MR_2 into the Cp_2MR^+ by protolysis.

The purpose of this thesis is to obtain an effective cocatalyst in metallocene catalyst for ethylene polymerization. We synthesized a salt of $Ph(Me)_2NH^+$ and anion obtained by the "topotactic" reduction of the two-dimensional host lattice system such as molybdenum disulfide (MoS_2) and tungsten disulfide (WS_2) and investigated the effect of this salt on catalytic activity of a metallocene catalyst, and influences of the guest cation content in the salt, the crystallite size of the salt, and the nature of anion obtained by the "topotactic" reduction for the ethylene polymerization. Moreover, the ethylene/1-hexene copolymerization with these catalyst systems was investigated.

---

†Catalysis and Polymerization Group, Yokkaichi Research Laboratory, TOSOH CORPORATION

2. Results and Discussion

2-1. Effect of "topotactic" reduction product of MoS_2 on catalytic activity of metallocene catalyst [2,3]

We synthesized $Ph(Me)_2NH^+$ intercalated MoS_2 and studied the effect of the compound on catalytic activity of metallocene catalyst and the influence of the $Ph(Me)_2NH^+$ content in the compound for ethylene polymerization. In ethylene polymerization, addition of this $Ph(Me)_2NH^+$ salts to the bis(indenyl)zirconium dichloride (Ind_2ZrCl_2)/triethylaluminum (Et_3Al) catalyst improves the catalytic activity per mmol of Ind_2ZrCl_2 and the catalytic activity increases with increasing amount of the cocatalyst. Poly(ethylene) and poly(ethylene-*co*-1-hexene) obtained with the metallocene activated by this cocatalyst have typical features such as narrow molecular weight distribution and narrow composition distribution like as polymers obtained with conventional metallocene catalysts. So, we propose that $Ph(Me)_2NH^+$ in the interlayer space of MoS_2, especially on the edges of layered structure of MoS_2 would activate neutral dialkylmetallocene into cationic monoalkylmetallocene by protonolysis and that the two-dimensional macroanions of MoS_2 would act as non-coordinating anions and supports for the obtained cationic species.

2-2. Effect of "topotactic" reduction product of WS_2 on catalytic activity of metallocene catalyst [4,5]

We synthesized $Ph(Me)_2NH^+$ intercalated WS_2 and studied the effect of this compound on catalytic activity of metallocene catalyst and the influence of the crystallite size of this compound in ethylene polymerization in comparison with the above $Ph(Me)_2NH^+$ intercalated MoS_2. In ethylene polymerization, addition of this $Ph(Me)_2NH^+$ intercalated WS_2 to the Ind_2ZrCl_2/Et_3Al catalyst enhanced drastically the catalytic activity in comparison to the $Ph(Me)_2NH^+$ intercalated MoS_2, which had smaller crystallite size than the $Ph(Me)_2NH^+$ intercalated WS_2. Poly(ethylene) obtained with the metallocene catalyst activated by addition of the $Ph(Me)_2NH^+$ intercalated WS_2 has typical features such as narrow molecular weight distribution like polymers obtained with conventional metallocene catalysts, indicating that the active species of this catalyst system was the cationic monoalkylmetallocene adsorbed on the edge site of the $Ph(Me)_2NH^+$ intercalated WS_2. The Zr loadings on the precipitate of the Ind_2ZrCl_2/Et_3Al catalyst activated by the $Ph(Me)_2NH^+$ intercalated WS_2 increased with decreasing crystallite size of the $Ph(Me)_2NH^+$ intercalated WS_2. However, the catalytic activity of the catalyst decreased drastically with the decreasing crystallite size, indicating that the decrease of the crystallite size led to the significant increase of inactive species for ethylene polymerization, probably the base-coordinated adducts.

3. Concluding remarks

i) The salt based on anion obtained by the "topotactic" reduction of the two-dimensional host lattice system, especially WS_2 is a significantly effective cocatalyst in metallocene catalyst for ethylene polymerization.
ii) The catalytic activity of this metallocene catalyst system depends on both the $Ph(Me)_2NH^+$ content in the interlayer space of this cocatalyst and the crystallite size of the cocatalyst.

Author's publications

[1] S. Yamada, A. Yano, US Patent 6372681 (2002).
[2] S. Yamada, A. Yano, M. Sato, T. Itoh, J. Mol. Catal. A, Chem. 200 (2003) 239-249.
[3] S. Yamada, A. Yano, M. Sato, Polymer Preprints, Japan Vol. 51, No. 8 (2002) 1595.
[4] S. Yamada, A. Yano, M. Sato, T. Itoh, J. Mol. Catal. A, Chem. in press.
[5] S. Yamada, A. Yano, M. Sato, Polymer Preprints, Japan Vol. 52 in press.

A Study of Magneto-Optical Recording using a High Numerical Aperture Lens and Short Wavelength Laser

Ariyoshi Nakaoki†
(Department of Material Science)

Keywords: Magneto-Optic, High density, Numerical aperture, Wavelength, Spot size, Sputtering, Noise level, Disk noise, Etching substrate, Reactive Ion Etching

1. Introduction

Because the recording density of an optical disc depends on the wavelength of the light source and the numerical aperture (NA) of an object lens, it becomes very important what optical parameter is chosen. After the fist announcement of an optical video disk in 1972, the recording density of an optical disc has been improved with shortening of the wavelength of laser and shifting NA of an object lens higher.

On the other hand, the magneto-optical (MO) disc was commercialized as a rewritable storage medium for computer peripheral apparatus in 1988. The development for high density recording has been achieved by adopting of a ZCAV system, a mark edge detection method, and a MSR (Magnetically Induced Super Resolution) medium which used an exchange coupled magnetic multilayered films and the total capacity of disc amounts to 10 or more times as compared with that of a first product. In the MO disc, several approaches for high density recording using a mean of a disc format or recording films have been reported, but very few approaches having examined the optical parameter of wavelength and NA have been reported.

Then, the main purpose of this paper is discussion about the possibility of high density recording in MO disc combined with a higher NA of objective lens and a shorter wavelength of a light source. As the 1st research, (1) the effect of NA of 0.85 is argued in the point of view of recording density. Here, the significant problem caused from the film stacking in the order of reverse or the reproducing of magneto-optical disc with a laser incidence from film side will be considered. Furthermore, the relationship between a small optical spot size by higher NA and a noise level during a reproducing is discussed. By 2nd research following it, (2) the shorter wavelength of 405 nm is applied and the upper limitation of recording density is considered when laser device of 405 nm is combined with objective lens of NA 0.85.

2. Experimental conditions

Figure 1 shows the experimental set up for achieving an effective NA of 0.85. The hemisphere lens made from quartz glass is assembled with keeping an optimum distance from the conventional objective lens of NA 0.6. The laser with wavelength of 650 nm was used in order to evaluate an effect of high NA optics and the laser of 405 nm is used for estimation of recording density. The MO disc for measurement has an almost same structure with a conventional disc. The recording film is deposited on a glass 2P substrate in the order of reverse and consists of the first dielectric layer, magnetic double layer of GdFeCo and TbFeCo materials, the thermal control layer of silver, the second dielectric layer and the reflective layer of silver. These recording films were covered by a polymer resin with thickness of 20 μm. The carrier signals and modulated signal in (1, 7)-RLL code were recorded on MO disc by magnetic field modulated (MFM) method.

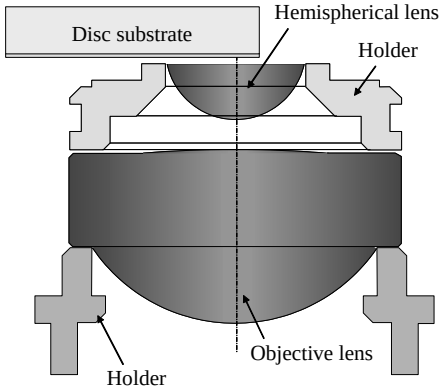

Fig. 1. A schematic drawing of the 2-elment objective lens for high NA of 0.85.

3. Results and discussion

The noise level during reproducing a MO disc with NA 0.85 optics was measured and was compared with the case of NA 0.55. It was found that the noise level of NA 0.85 was worse than that of NA 0.55 and the

† Sony Corporation

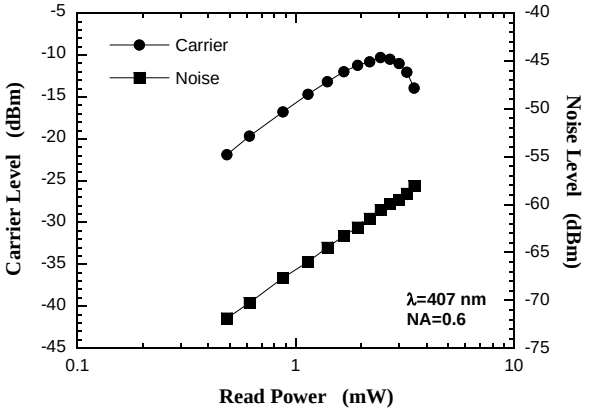

Fig. 2. The reproducing laser power dependence of carrier level and noise level of MO disc.

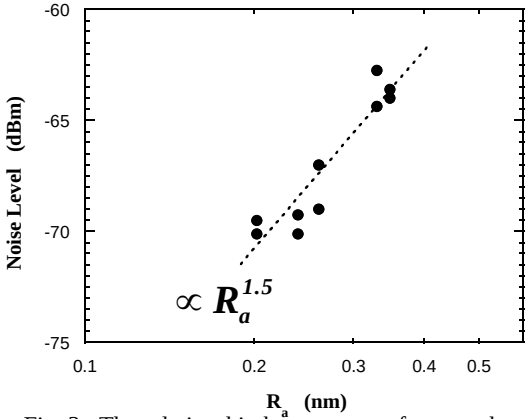

Fig. 3. The relationship between a surface roughness Ra and a disc noise level.

differences were obtained 3 dB at mirror part of substrate, 5 dB at groove part, respectively. In order to investigate the cause of the noise increase, a reproducing power dependence of noise level was measured as shown in Fig. 2. The dependence of carrier level is also shown in this figure. It is obvious that the noise level is simply proportional to reproducing power, but the carrier level is not in the higher power region than 2.5 mW. From this result, it is considered that a fluctuation of Kerr rotation angle which affects to the carrier level is not the main cause of noise increase. We predict that the noise level is determined by the fluctuation of polarization characteristic which depends on a laser incident angle at disc surface. The laser incident angle will be changed easily by roughness of disc surface. Then, we investigated the relation between a surface roughness Ra and noise level. The surface roughness Ra is measured by the atomic force microscope (AFM). The result is shown in Fig. 3 and it is found that the noise level is proportional to the 1.5th power of Ra. Because the relationship between the surface roughness of substrate and reproducing noise level was obvious, we could conclude that the main cause of reproducing noise was the fluctuation of polarization characteristic which was strongly concerned with the disc surface roughness. It is also considered that the noise will increase in the case of reproducing with higher NA objective because relative roughness will become large if spot size becomes small. It becomes a significant problem as to high density recording by adopting a small laser spot. Therefore, in this research, we adopted UV irradiation method as a pre-treatment method of disc, reactive ion etching (RIE) method as a disc mastering process in order to create a low noise disc with a smooth surface. Consequently, it succeeded in improving 5dB or more of noise levels in a groove part. The read/write performances on this improved disc were measured with several optical parameters. The combination of NA (0.55, 0.85) and wavelength (655 nm, 405 nm) were used as optical parameters. The performance of disc is estimated by its jitter value which means the fluctuations of signal waveform with varying a recording density. And then, the critical recording density is determined according to a jitter criterion of 12.5 %. The experimental results are shown in Fig. 4. It is clear that critical track pitch and bit length are proportional to the spot size which is calculated with (0.8*wavelength/NA). It turns out inevitably that recording density is proportional to the 1/2nd power of spot size. The maximum recording density of 20 Gbit/inch^2 was achieved if the optical parameter of NA 0.85 and wavelength of 405 nm was used. This recording density corresponds to 5 times of that in the case of NA 0.6 and wavelength of 650 nm, and it is considered to be appropriate from a viewpoint of an optical parameter.

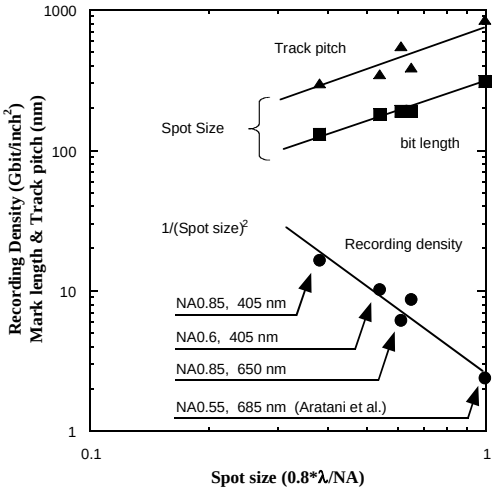

Fig. 4. The comparison of achieved recording density with several optical parameters.

5. Conclusion

The possibility of high density recording in MO disc combined with an objective lens of NA 0.85 and a short wavelength laser of 405 nm was evaluated. It is found that the disc noise caused by surface roughness becomes significant if a small spot size of laser is used for reproducing an optical disc. Therefore, the low noise disc with a smooth surface is the indispensable condition for high density recording combined with higher NA lens and shorter wavelength laser. We succeeded in making a low noise disc and could achieve a high density recording of 20 Gbit/inch^2 by adopting an objective lens of NA 0.85 and wavelength of 405 nm.

Development Research of Novel Antioxidants For Antiatherogenic Agent

Kunio Tamura †

Key Words: Antioxidants, Lipid Peroxyl Radical, LDL, Atherosclerosis, WHHL Rabbit, Antiatherogenic Agent, Drug Design, Synthesis, Structure Activity Relationship, BO-653

1. Introduction

Recently, many lines of evidence, based on studies in cell culture and in experimental animal models, suggest that the oxidative modification of low-density lipoprotein (LDL) has a critical role in the development of atherosclerosis. In this research, two types of antioxidants which prevent the oxidative modification of LDL were designed, and the aim of this research is inventing a new antioxidant useful as an antiatherogenic agent in clinical from the structure activity relationship study.

2. Results and Discussion

2-1. Synthesis of Aniline-type Antioxidants and Their Antioxidant Activity

Since the amount of LDL metabolism via the scavenger receptor in a macrophage becomes less when the oxidative modification of LDL is prevented by antioxidants, the absolute quantity of native LDL will increase theoretically. Therefore, the drug that prevents the oxidative modification of LDL and reduces plasma LDL by prevention of cholesterol biosynthesis is rational. The author focused attention on the antioxidant action of the aniline derivatives that are the related compound of phenol known as an antioxidant. Thus many types of aniline derivatives that possess antioxidant activity and inhibitory effect on cholesterol biosynthesis were designed and synthesized. From the consideration of their structure activity relationship, it was found that the aniline-type derivatives were a quencher of superoxide radical (O_2^-) which is one of the oxygen radicals. Since it is not clear whether they are effective for prevention of atherosclerosis, the compound with the highest distribution to the blood of an atherosclerosis animal model was chosen and its antiatherogenic effect was investigated. However, the selected compound **1** was invalid in the animal model, although probucol, a selective antioxidant for a lipid peroxyl radical, showed antiatherogenic effect. Thus it resulted in the conclusion that it is important to scavenge a lipid peroxyl radical for effective inhibition of atherosclerosis progression.

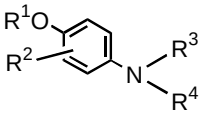

Aniline derivatives

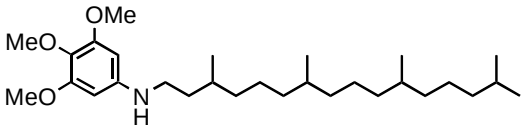

1

† Chugai Pharmaceutical Co., Ltd.

2-2. Synthesis of Dihydrobenzofuranol-type Antioxidants and Their Antioxidant Activity

From the result of the aniline derivatives, the author started a new drug design for an ideal antioxidant by compensating disadvantage of α-tocopherol, the most potent antioxidant *in vivo*. Then, the author hypothesized that the requirements as a LDL antioxidant would be possessing stronger antioxidant activity than α-tocopherol, demonstrating antioxidant activity in the core of LDL particle, and negating the character as a prooxidant which α-tocopherol possesses. The author concluded that the rationally-designed new antioxidant should have the following characteristics.

1) High hydrogen-donating activity and low prooxidant activity of its resulting radical intermediate
2) Localization inside the core of the LDL particle
3) Sufficient delivery to LDL and vascular vessel wall

As a structure that can realize the above, the author performed the design and synthesis of dihydrobenzofuranol derivatives, and succeeded in clarifying the strong antioxidant activity. Moreover, as the technique of evaluating the localization to LDL, the author succeeded in building the strategy for screening the optimal LDL antioxidant by performing the oral administration using the WHHL rabbit that is a typical animal model for atherosclerosis. As the result of the above research, the author selected 4, 6-di-*tert*-butyl-2,3-dihydro-2,2-dipentyl-5-benzofuranol **2** as an optimal compound, and clarified the potent LDL antioxidant action as a clinical candidate for an antiatherogeic agent.

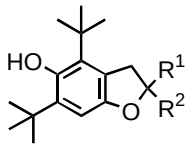

Dihydrobenzofuranol derivatives

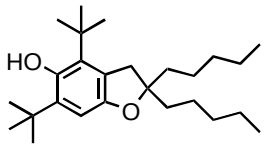

2 (BO-653)

3. Conclusions

In this research, the author performed the design and synthesis of the aniline derivatives and the dihydrobenzofuranol derivatives as new antioxidants, and showed the structure activity relationship of their antioxidant activities. Moreover, the author showed that **2** (BO-653) possesses the potent antioxidant activity which is required for an effective antiatherogenic agent. BO-653 is a promising candidate as a new antiatherogenic agent in clinical. The author expects that the potential of antioxidants to cardiovascular diseases like atherosclerosis is clarified by the clinical trial currently performed in the U.S.

Author's Publications

[1] Tamura, Kunio; Kato, Yoshiaki; Ishikawa, Akira; Kato, Yasuharu; Himori, Motomu; Yoshida, Mitsutaka; Takashima, Yoshiaki; Suzuki, Tsukasa; Kawabe, Yoshiki; Cynshi, Osamu; Kodama, Tatsuhiko; Niki, Etsuo; Shimizu, Makoto, Design and synthesis of 4,6-di-*tert*-butyl-2,3-dihydro-5-benzofuranols as a novel series of antiatherogenic antioxidants. *J. Med. Chem*. **2003**, *46*, 3083-3093.

[2] Tamura, K.; Kato, Y.; Ishikawa, A.; Kato, Y.; Himori, M.; Yoshida, M.; Cynshi, O.; Higashida, A.; Aono, R.; Ohba, Y., Design and synthesis of novel dihydrobenzofuranol antioxidants. Book of Abstracts, 214th ACS National Meeting, Las Vegas, NV, September 7-11 (1997), MEDI-218.

[3] Tamura, K.; Kato, Y.; Yoshida, M.; Cynshi, O.; Ohba, Y., Preparation of 4-alkoxy-2,6-di-t-butylphenol derivatives as antiarteriosclerotic agents. WO94/08930.

[4] Kato, Y.; Tamura, K.; Ohba, Y.; Kawabe, Y.; Cynshi, O., Preparation of aniline derivatives as low-density lipoprotein inhibitors. WO91/11994.

Surface properties of inorganic/organic hybrids prepared by sol-gel method and application to novel heat-resistant materials

Takuya Shindou†

Keywords: sol-gel, organic/inorganic hybrid, polydimethylsiloxane, PDMS, surface morphology, AFM, electrical insulation, thermal conductivity, heat-resistance

1.Abstract

Polydimethylsiloxane(PDMS)-based inorganic/organic hybrid films were prepared by sol-gel method using silanol-terminate PDMS and metal alkoxide as starting materials. Surface morphology of the hybrids was examined in terms of contact angle of water and a tapping-mode Atomic Force Microscopy (AFM). A phase separation of hydrophilic and hydrophobic areas appeared on the surface of the hybrid films heat-treated at 150℃. The phase separation disappeared with increasing heat-treated temperature. The hybrid film heat-treated at 300℃ shows a homogeneous surface and indicates a relatively high contact angle of water, ～115° The PDMS-based hybrid film exhibited an excellent toner peeling capability, suggesting its practical use in the xerographic printers. Electrical and mechanical properties of PDMS-based inorganic/organic hybrids have been studied. The PDMS-derived hybrid shows an excellent electrical insulation property of more than $10^{10}\Omega \cdot m$ even at 200℃. By mixing filler with the hybrid sol, a functionalized sheet could be made. The hybrid mixed with aerosil and boron nitride yields a good mechanical property and the hybrid mixed with alumina shows a high thermal conductivity beyond 5 W/m・K. The hybrids are expected to have potential for heat-resisting electrical insulating materials.

2.Introduction

In the field of electro-photographic printing, the demand for a higher quality and speedy print has increased. It requires to replace traditional components with good performance ones for that purpose. The author has been making an effort to apply inorganic/organic hybrids to xerographic printer component, with the expectation that the property of those hybrids can be controlled by tailoring the nanostructure. The PDMS-based hybrids have not only properties such as flexibility and thermal stability[1)-4)] but also potential for water-repellency as expected from the nature of dimethylsilicon units. The structure and mechanical properties of PDMS-based hybrids have been clarified by various research papers[5)-7)], however, there are very few studies on shortening the film preparation and controlling the surface properties. They are important factors when applied to the material of xerographic components. In this work, the effect of heat-treatment temperature and inorganic/organic molar ratio on the film surface properties was examined. Furthermore, the evaluation of applicability of the hybrid to the practical use was carried out in terms of the so-called "toner offset."

In addition to the capability as a thermal-fixation roll of xerographic printer, PDMS-based hybrids have great potential for novel electrical insulating materials because the hybrids have the good properties of heat-resisting, electrical insulating and elasticity. Recently, heat generation from central processing units is rapidly getting large because the electronics device is moving into downsizing and high-speed processing. The demand of heat-resistive electronic materials in high temperatures is increasing. The electrical properties such as volume resistivity, relative permittivity and loss tangent of the hybrid sheets were examined up to 200℃. Because a lot of fillers can be introduced into the hybrid sol, functionalized hybrid sheets have developed in this work. The thermal conductivity and mechanical properties of the hybrid sheet were examined.

3.Surface properties of TIP(Ti-isopropoxide)-PDMS-based inorganic/organic hybrid

The PDMS-based hybrids have a smooth surface about 10nm level. The phase images of hybrid films by AFM are shown in Fig.1. The films were prepared by changing the molar ratio of PDMS to TIP from 0.2 to 0.35 and heat-treated at 150℃. It can be seen that the image changes for the molar

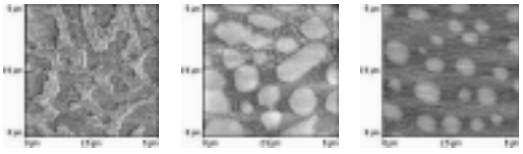

PDMS/TIP=0.2 PDMS/TIP=0.3 PDMS/TIP=0.35

Fig. 1. Phase image of AFM for PDMS-based hybrids heat-treated at 150℃.

† Advanced Technology Research and Development Division, Suzuka Fuji Xerox Co., Ltd.,

ratio; in the case of the low ratio of 0.2, separated continuous two domains are observed and they change into a clear island-shaped spot when the molar ratio increases. The spots are considered to be more hydrophilic than the rest or matrix region and to be rich in titania or TIP species leading to a large contact angle of water with increasing the molar ratio. The phase images of the hybrid films heat-treated at 300℃ exhibit a featureless or homogeneous surface at any PDMS/TIP ratio and the films show a hydrophobic surface property.

4.Electrical properties of TIP-PDMS-based inorganic/organic hybrid

Figure 2 shows the volume resistivity of the TIP-PDMS-based hybrid films at room temperature and 200℃. The hybrid films show an excellent electrical insulation property of more than $10^{10}\Omega \cdot m$ even at 200℃. The properties of relative permittivity ($\varepsilon r'$) below 5 and the loss tangent ($\tan\delta$) below 4×10^{-4} at 200℃, suggesting that the hybrid has high potential for electrical insulating material. It has been found that the dependence of dielectric properties on temperature (room temperature to 250℃) or frequency (40Hz to 400kHz) of the hybrid film shows no sign of dielectric relaxation.

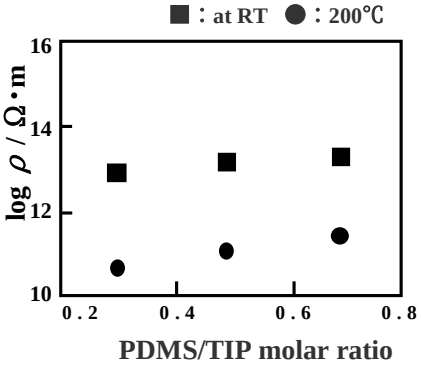

Fig. 2. Change of volume resistivity of hybrid for the molar ratio of PDMS to TIP.

5.PDMS-based inorganic/organic hybrid sheet and functionalization

Figure 3 show the appearance of ZTP(Zr-propoxide)-PDMS-based hybrid sheet. It has been also found that the sheet is very heat-resistive. By mixing filler with the hybrid sol, a functionalized sheet can be made. Zr tetra-propoxide (ZTP)-PDMS-derived hybrid mixed with aerosil and boron nitride yields a good mechanical property and the hybrid mixed with alumina shows a high thermal conductivity beyond 5 W/m・K.

Fig. 3. Appearance of ZTP-PDMS-based hybrid sheet.

6.Conclusion

The surface morphology of PDMS-based inorganic/organic hybrid films has been examined. These results give a promising application of PDMS-based hybrids to novel parts of the xerographic printer. And the hybrid mixed with functionalizing fillers shows high potential for heat-resisting, thermal conducting and electrical insulating materials.

7.References

1) H. Shmidt, New Type of Non-Crystalline Solids between Inorganic and Organic Materials, J. Non-Cryst. Solid, 73, pp.681-191 (1985).
2) G. L. Wilkes, B. Orler and H. Huang, Ceramer : Hybrid Materials Incorporating Polymeric/Oligomeric Species into Inorganic Glasses utilizing a Sol-Gel Approach, Polym. Prep., 26[2], pp.300-302 (1985).
3) H. Huang, B. Orler and G. L. Wilkes, Structure-Properties Behavior of New Hybrid Materials Incorporating Oligomeric Species into Sol-Gel Glasses.3. Effect of Acid Content, Tetraethoxysilane Content, and Molecular Weight of Poly(dimethylsiloxane), Macromolecules, 20[6], pp.1322-1330 (1987).
4) Y. J. Chung, S. –J. Ting and J. D. Mackenzie, "Rubbery Ormosils"; pp.981-986 in Better Ceramics Through Chemistry IV, Proceedings of the Materials Research Society Symposium 180 (San Francisco, CA, April 1990). Edited by B. J. J. Zelinski, C. J. Brinker, D. E. Clark, and D. R. Ulrich. Materials Research Society, Pittsburgh, PA, (1990).
5) J.D. Mackenzie, Q. Huang, and T. Iwamoto, Mechanical Properties of Ormosils, J.Sol-Gel Sci. and Tech. 7, pp.151-161 (1996).
6) J.D. Mackenzie, J.Sol-Gel Sci. and Tech., Structures and properties of ormosils, 2, pp.81-86 (1994)
7) S. Katayama, Y. Kubo and N. Yamada, Characterization and Mechanical Properties of Flexible Dimethylsiloxane-Based Inorganic/Organic Hybrid, J. Ceram. Soc. 85(5), pp.1157-1163 (2002).

Author's Publications

[1] T. Shindou, S. Katayama, N. Yamada and K. Kamiya, Surface properties of Polydimethylsiloxane-Based Inorganic/Organic Hybrid Films Deposited on Polyimide Sheets by the Sol-Gel Method, J.Sol-Gel Sci. and Tech., 27, pp.15-21 (2003)
[2] T. Shindou, H. Konishi, S. Nakamura and K. Kamiya, ZTP-PDMS derived organic/inorganic hybrid materials, TECHNICAL REPORT OF IEICE., OME2003-102(2003-11), SHINGAKUGIHOU, Vol.103, No.441 , pp.25-29 (2003)

Study on Spontaneous Polymerization Mechanism of Electron-accepting Substituted Quinoid Compounds with Electron-donating Vinyl Monomers

Yukihiro Mitsuda
(Polymer Synthesis Lab., Division of Material Science)

Keywords: Polymerization Mechanism, Electron-Accepting Quinoid Compounds, Electron-donating Vinyl Monomers, Gauche- and Trans-form Zwitterionic Intermediates

Introduction

Spontaneous reactions of electron-accepting olefin monomers with electron-donating ones gave alternating copolymers and/or homopolymers. To explain these spontaneous reactions, Hall and coworkers have proposed the "bond-forming initiation theory", where tetramethylene intermediates, which are diradical or zwitterionic depending on the nature of the substituents on the olefins, are formed between electron-accepting olefins and electron-donating ones, and diradical intermediate leads to an alternating copolymer and the zwitterionic one leads to a homopolymer. This theory has been extended to the spontaneous reactions of diolefins and quinoid compounds. Previously, Iwatsuki *et al.* reported that spontaneous reaction of symmetrically electron-accepting substituted quinoid compound, 7,7,8,8-tetracyanoquinodimethane (TCNQ), with electron-donating vinyl monomer, styrene, proceeded via diradical intermediate to give alternating copolymer. In this work, spontaneous reactions of unsymmetrically substituted quinoid compound, 1-(2,2-dimethyl-1,3-dioxane-4,6-dione-5ylidene)-4-(dicyanomethylene)-2,5-cyclohexadiene (QM-1) with electron-donating vinyl monomers, *p*-, α- and β-substituted styrenes (RSt: R = pOMe, pMe, pH, pAcO, pCl, pCOOMe, pCN, αMe, αPh, βMe, βPh), butyl vinyl ether (BVE) and 2-methylene-1,3-dioxepane (MDOP) were investigated to elucidate reaction mechanism.

Experimental Section

A given amount of QM-1 and chloroform were placed in a glass ampoule, and into the resulting solution was added a solution containing a given amount of electron-donating vinyl monomers in chloroform. After stirring at a given temperature for a given hour, the reaction mixture was poured into a large amount of hexane to deposit a polymeric product as a hexane-insoluble fraction. The polymeric product was purified by dissolution-reprecipitation method using chloroform as a solvent and hexane as a precipitant, respectively, and dried under reduced pressure until the constant weight was attained. The supernatant was placed under reduced pressure to remove a solvent and give a residue as a hexane-soluble fraction, which was dried under reduced pressure until the constant weight was attained. The polymeric and residual products were characterized by ^{1}H NMR, ^{13}C NMR and IR spectroscopies, GPC, and elemental analysis.

Results and Discussion

Spontaneous Reaction of QM-1 with pMeOSt

The polymer obtained as a hexane-insoluble fraction was determined to be random copolymer of trisbstituted quinodimethane, 7-(4-methoxyphenyl)-8,8-dicyanoquinodimethane, and QM-1 units. On the other hand, residual product obtained as a hexane-soluble fraction was to be unreacted QM-1 and one-to-one cycloadduct (Cycloadduct) of methylene Meldrum's acid (MM) and pMeOSt. To obtain some information

about the reactive intermediate formed in the system, the spontaneous reactions of QM-1 with pMeOSt in the presence of TEMPO as radical inhibitor or methanol as ionic one were investigated. In the presence of TEMPO, the copolymer yield and molecular weight were lower compared with the corresponding one obtained in the absence of TEMPO. These results indicated that the copolymer obtained as a hexane-insoluble fraction was formed by radical mechanism. In the presence of methanol, one-to-one-to-one adduct of QM-1, pMeOSt, and methanol was isolated. This strongly indicated that a zwitterionic intermediate was formed in spontaneous reaction of QM-1 with pMeOSt. On the basis of these results, the mechanism for spontaneous reaction of QM-1 with pMeOSt was proposed as shown in Scheme that the cyclobutane ring was formed via gauche-form zwitterionic intermediate, and then it cleaved via metathesis process to generate QM-2 and MM, the former of which copolymerized with QM-1 to give a random copolymer and the latter of which reacted with pMeOSt to form Cycloadduct.

Spontaneous Reactions of QM-1 with BVE and with MDOP

In spontaneous reaction of QM-1 with BVE, the polymer obtained as a hexane-insoluble fraction was determined to be a random terpolymer consisted of trisubstituted quinodimethane, 7-butoxy-8,8-dicyanoquinodimethane (QM-2), QM-1, and BVE units. The hexane-soluble product was to be one-to-one cycloadduct of MM and BVE. These results indicated that the mechanism for spontaneous reaction of QM-1 with BVE was similar to QM-1/MeOSt system. On the other hand, in spontaneous of QM-1 with MDOP, the polymer was an alternating copolymer of QM-1 and MDOP. This result was different from one of QM-1/BVE system. Thus, it suggested that the substitution mode of comonomer influenced to reaction mechanism, that is, as MDOP is α,α-disubstituted olefin, no cyclobutane ring was formed, and then isomerization to trans-form zwitterionic intermediate took place.

Spontaneous Reactions of QM-1 with RSt

For the uses of pCOOMeSt, pCNSt, αPhSt, and βPhSt, no spontaneous reaction occurred because of weaker electron-donating or more bulky vinyl monomers. Spontaneous reaction of QM-1 with αMeSt gave an alternating copolymer. This result was same one of QM-1/MDOP system. In the case of RSt (R = pMe, pH, pOAc, pCl, βMe), the obtained polymers were determined to be random terpolymer including trisubstituted quinodimethane (QM-2) unit. As these results, the reaction mechanism was affected by the nature, bulkiness, and position of substituent.

Conclusions

Spontaneous reactions of quinoid compounds with electron-donating vinyl monomers were investigated. It was found that polymerization proceeds via zwitterionic intermediate, which existed in gauche or trans-forms, the former of which gave a random copolymer and the latter of which gave an alternating copolymer.

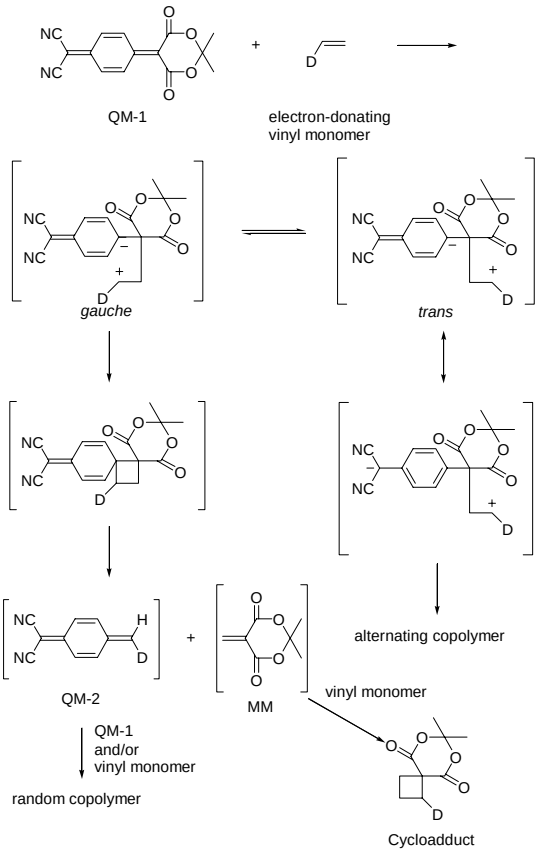

Scheme

Author's publications

1) Y. Mitsuda, T. Fujikawa, T. Uno, M. Kubo and T. Itoh, *Macromolecules*, **2003**, *36*, 1028.
2) Y. Mitsuda, S. Kawaguchi, T. Uno, M. Kubo and T. Itoh, *Macromolecules* **2004**, *37*, 1251.
3) S. Kawaguchi, Y. Mitsuda,, T. Uno, M. Kubo and T. Itoh, *Kobunshi Ronbunshu* in press
4) Y. Mitsuda, T. Fujikawa, K. Nakasaka, T. Uno, M. Kubo and T. Itoh, *J. Polym. Sci. Part A Polym. Chem.* to be submitted.

Study on AlN epitaxial films grown by MOVPE method and their applications

Tomohiko Shibata†

Keywords: AlN, III-V nitride, MOVPE, Crystal Quality, Dislocation, SAW

1. Introduction

Al-rich III-V nitrides have a great potential for future optical devices in ultraviolet region, including light emitting diodes (LEDs), laser diodes (LDs) and photodetectors, due to their wide band gap. In particular, AlN has piezoelectricity and the widest direct band gap (6.2eV) of the III-V nitride materials, so that the realization of high-quality AlN epitaxial films can widely extend application fields of III-V nitride materials. So far, fewer researches on AlN epitaxial growth have been reported than on GaN epitaxial growth due to large difficulties in AlN growth. In this study, I realized high-quality AlN epitaxial films on several single-crystalline substrates using a metal organic vapor phase epitaxy (MOVPE) method and I made it clear that the AlN epitaxial films had great potentials for various applications including optoelectronic devices, electronic devices and surface acoustic wave (SAW) devices.

2. Application for optoelectronic and electric devices

(0001)-faced AlN epitaxial films on (0001)-faced sapphire or 6H-SiC substrates are promising as templates for the AlGaN growth that can be applied to wide range of semiconductor devices.

First of all, I achieved crackless high-quality AlN epitaxial films with an atomically flat surface on both substrates as shown in Fig.1. It is characteristic features that the AlN epitaxial films have narrow X-ray rocking curve (XRC) profiles for (0002) plane with full width at half maximum (FWHM) values equal to less than 100 arcsec. A dislocation density of the AlN epitaxial films is as low as $1x10^{10}/cm^2$, which is a lower value than ever reported, and most of dislocations consist of edge-type ones[1,2].

Next, I found the effect of AlN templates for AlGaN growth. The overgrown AlGaN films have no cracks in all AlN molar fraction range. XRC FWHM values for (0002) plane of the AlGaN epitaxial films are equal to less than 200 arcsec, which is least values ever reported[3,4]. In the case of an overgrown GaN film, in particular, its dislocation density reaches as low as

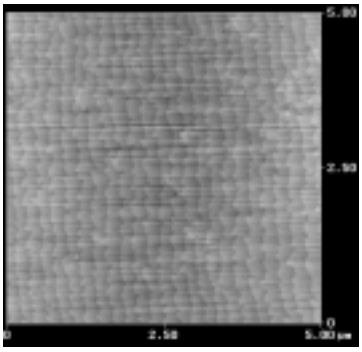

Fig. 1 AFM surface image of AlN film in the region of 5x5μm on sapphire.

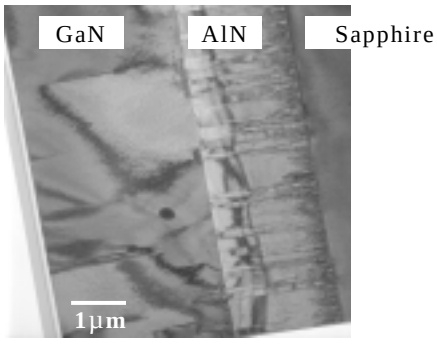

Fig. 2 Bright-field Cross-section TEM image.

† NGK INSULATORS, ltd.

$4x10^8/cm^2$ and a dislocation density dropped by less than a tenth from AlN to GaN as shown in Fig.2[5,6]. It is thought that the phenomena of the restraint of crack generation and the drastic reduction of dislocations are caused by a compressive stress due to larger in-plane lattice constants of the overgrown AlGaN layer than that of the underlayer AlN.

The improvement of crystal qualities of the overgrown AlGaN results in improving some device performances, such as luminous efficiency of LEDs, electronic properties of HEMT devices and so on.

3. Application for SAW devices

In order to realize SAW devices, a $(11\bar{2}0)$-faced AlN epitaxial film on a $(10\bar{1}2)$-faced sapphire substrate is the most promising combination due to its modest electromechanical coupling coefficient (1%) and its high SAW velocity (6000m/sec). Therefore, the AlN/sapphire is a promising candidate for SAW devices operating in a GHz band, which is required for current wireless communication systems. However, there have been remained some problems to degrade crystal qualities of the AlN film, for instance, inverted twins which caused a reduction of the value of electromechanical coupling coefficient. Systematic optimization of the growth conditions of the AlN was carried out during MOVPE in order to extract the above-mentioned potential properties.

The use of off-angle $(10\bar{1}2)$-faced sapphire substrates, in which the surface plane was tilted towards $[1\bar{1}01]$ sapphire direction, was shown to effectively restrain the generation of the inverted twins. The results of AlN grown on a round-shaped $(10\bar{1}2)$-faced sapphire support that an off angle with specific direction is effective in improving crystal qualities as well as restraining inverted twin[7,8]. Furthermore, SAW filters at 2.4GHz packaged into 5x7mm size were reliably realized using the optimized AlN on the off-angle sapphire substrates[9].

4. Conclusion

High-quality AlN epitaxial films were realized using MOVPE method on a (0001)-faced sapphire, a (0001)-faced 6H-SiC substrates and a $(10\bar{1}2)$-faced sapphire. As a result, potentials of AlN can be extracted and it is found that the AlN epitaxial films are useful for templates of high-quality AlGaN growth and substrates for SAW devices.

Author's publications

[1] T. Shibata, K. Asai, T. Nagai, S. Sumiya, M. Tanaka, O. Oda, H. Miyake and K. Hiramatsu; Materials Research Society Symposium Proceedings, Vol. 693 (2002) 541.
[2] T. Shibata, K. Asai, S. Sumiya, M. Mouri, M. Tanaka, O. Oda, H. Katsukawa, H. Miyake and K. Hiramatsu; Phys. Stat. Sol (c) Vol. 0 No. 7, (2003) 2023.
[3] Y. Kida, T. Shibata, H. Naoi, H. Miyake, K. Hiramatsu and M. Tanaka; Phys. Stat. Sol. (a) Vol. 194 No. 2, (2002) 498.
[4] Y. Kida, T. Shibata, H. Miyake and K. Hiramatsu; Jpn. J. Appl. Phys. Vol. 42 (2003) L572.
[5] T. Shibata, Y. Kida, H. Miyake, K. Hiramatsu, Y. Hori, K. Asai, T. Nagai, S. Sumiya, M. Tanaka and O. Oda; Compound Semiconductors 2001 (Inst. Phys. Conf. Ser. No. 170) 795.
[6] T. Shibata, Y. Kida, H. Miyake, K. Hiramatsu, K. Asai, T. Nagai, S. Sumiya, M. Tanaka and O. Oda; Materials Research Society Symposium Proceedings, Vol. 693 (2002) p.219.
[7] T. Shibata, K. Asai, Y. Nakamura, M. Tanaka, K. Kaigawa, J. Shibata and H. Sakai; Journal of Crystal Growth Vol. 229 (2001) 63.
[8] T. Shibata, Y. Hori, K. Asai, Y. Nakamura, M. Tanaka, K. Kaigawa, J. Shibata and H. Sakai; IPAP Conf. Series Vol. 1, (2000) 981.
[9] T. Shibata, Y. Hori, K. Asai, Y. Nakamura, M. Tanaka, K. Kaigawa, J. Shibata and H. Sakai; 2000 IEEE Ultrasonics Symposium Proceedings, (2000) 287.

The improved component materials using Rare Earths for SOFCs through the newly devised synthesis process and chemical composition.

Eisaku Suda †
(Materials Science)

Keywords: Sintering Characteristics, Coprecipitation, Rare Earth, Cerium Oxide, SOFC

Abstract

In this study, the synthesis process and chemical composition were investigated mainly in order to prepare the appropriate component materials using Rare Earths for SOFCs. Then the physical properties and some advantages have been clarified here.

For electrolyte, the low-temperature sinterable RE-doped ceria powders (fluorite) has been developed using a newly-devised heat-treatment process in the coprecipitation method. This powder shows the lowest value in the reported sintering temperatures of rare earth metal-doped ceria powders: Relative densities ≥ 94%, where sintered ceramics can provide gastightness, was attained for this new powder after heating at temperatures ≥ 1000°C (Fig.1). To lower densely-sintered temperature, use of sintering aids is undesirable because such aids may damage other cell components. The present low-temperature sintering characteristics of the electrolyte without sintering aids are quite attractive in view of the problems associated with the SOFC fabrication process.

The crystal structure, sintering characteristic, electrical conductivity and thermal expansion of $Gd_xTi_2O_{7-\delta}$ pyrochlores ($1.72 \leq x \leq 2.10$) have been measured and discussed as electrolytes in the high-temperature solid oxide fuel cells. These materials showed the indication of structural disorder with increasing A-site deficiency. Sintering characteristics of the pyrochlores promoted by A-site deficiency. The pyrochlores showed linear thermal expansion behavior in air and in the H_2 atmosphere, and with increasing A-site deficiencies, their TEC values decreased and were close to that of YSZ electrolyte. The electrical conductivity of these materials was slight lower than acceptable as the electrolyte in SOFC with high performance. In addition, the A-site deficiency in the pyrochlores caused an appearance of electronic conduction at high temperature under the reducing atmospheres. Thus, this problem remains to be solved. From the viewpoints of these properties, when it is

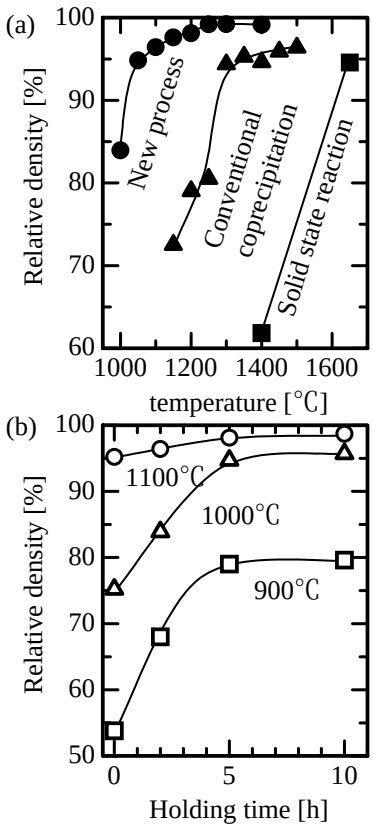

Fig.1 (a) Relative density of the $Ce_{0.9}Gd_{0.1}O_{1.95}$ (CGO) powders as a function of temperature, where the holding time at the highest temperature is 2h. (b) Relative density of new CGO as a function of holding time with a parameter of heating temperature.

† ANAN KASEI CO.,LTD.

considered the $Gd_xTi_2O_{7-\delta}$ pyrochlores for use as an electrolyte in the high-temperature SOFC, an enhancement of their electrical conduction for oxide-ion and a prevention of their electronic conduction at high temperatures under reducing atmospheres are necessary.

For anode, the preparation process and anodic properties for NiO-CGO powder were studied. Single cell tests on SOFC with anodes made from various NiO-CGO powders showed that anode polarization for spray dry was lowest. Overall, NiO-CGO prepared by spray dry (SD) gave the best result. SD as a starting powder had narrow particle size distributions. The Ni and CGO particles in the microstructure of SD showed good-connections between Ni-Ni, CGO-CGO and Ni-CGO particles were formed in the anodes. The appropriate Ni content in this system should be investigated in order to lower the sintering temperature of anode because NiO particles could prevent the sintering of HT-CGO particles.

For current collector, the properties of the $La_{0.6}AE_{0.4}MnO_3$ perovskites and $La_{0.6}AE_{0.4}MnO_3$-Mn_3O_4 composites (AE = Ca and Sr), have been evaluated as potential electric current collectors between the cathode and the interconnect in the high-temperature SOFC. The results can be summarized as follows; For $La_{0.6}AE_{0.4}MnO_3$ perovskites, $La_{0.6}AE_{0.4}MnO_3$ perovskites are not appropriate as electrical current collectors, because of a large difference in TECs between $La_{0.6}AE_{0.4}MnO_3$ and YSZ. For $La_{0.6}AE_{0.4}MnO_3$-Mn_3O_4 composites, (1) The TECs of the composites approached that of YSZ electrolyte at around 50 vol% Mn_3O_4, and the dense composites showed no anomalous thermal expansion behavior. (2) The manganese oxide addition greatly enhanced the sintering characteristics of the perovskites. It can be concluded that the dense $La_{0.6}AE_{0.4}MnO_3$–Mn_3O_4 composites are appropriate as potential electric current collectors in the high-temperature SOFC.

For interconnector, Li-doping of $La_{1-x}Sr_xCrO_3$ was an effective way of enhancing the sintering characteristics. The fine powders made by the Pechini method showed lower sintering characteristics when they were compared to those made by the solid-state technique. The solubility limit of Li element decreases with increasing Sr-content in the perovskites. Although the TECs of Sr-doped lanthanum chromites should be controlled by Sr-content, there is a serious problem in the fact that Sr cannot be included as solid solution at higher concentration. Improvements of TEC control and sintering have to be achieved for using as a separator of SOFC.

So many materials and fabrication methods for SOFC have been investigated in these thirty years. There, however, still remain many problems to be solved to obtain a high performance for SOFCs. The results of this work would inspire the future research and developments of SOFCs.

Author's publications

(1) Rhodia Electronics & Catalysis and Anan Kasei ; from a leadership in high purity rare earth compounds to a leadership in high performance rare earth based products., P. Macaudiere, B. Pacaud and E. Suda, *Rare Earths*, 39(2001)71-76.

(2) Low-temperature sinterable $Ce_{0.9}Gd_{0.1}O_{1.95}$ powder synthesized through newly-devised heat-treatment in the coprecipitation process, E. Suda, B. Pacaud, Y. Montardi, M. Mori, M. Ozawa and Y. Takeda, *Electrochemistry*, 71[10](2003)866.

(3) Electrical and thermal properties of dense $Ce_{1-x}RE_xO_{2-\delta}$ electrolyte using low-temperature sinterable powder ($0 \le x \le 0.2$, RE=Y, Sm, Gd), E. Suda, B. Pacaud, Y. Montardi, M. Mori, and Y. Takeda, *Material Research Society of Japan*, in press.

(4) Compatibility of $Gd_xTi_2O_7$ pyrochlores ($1.72 \le x \le 2.0$) as electrolytes in high-temperature solid oxide fuel cells, M. Mori, G. M. Tompsett, N. Sammes, E. Suda and Y. Takeda, *Solid State Ionics*, 158(2003)79-90.

(5) Microstructure and anodic properties of Ni-$Ce_{0.9}Gd_{0.1}O_{1.95}$ (CGO) cermets using sinterable CGO powder, E. Suda, B. Pacaud, Y. Montardi, M. Itagaki, S. Ohara and Y. Takeda, *American Ceramic Society*, in press.

(6) Application of $La_{0.6}AE_{0.4}MnO_3$ (AE=Ca and Sr) to electric current collectors in high-temperature solid oxide fuel cells, M. Mori, N. M. Sammes, E. Suda and Y. Takeda, *Solid State Ionics*, 164(2003)1-15.

(7) Sintering characteristics and thermal expansion behavior of Li-doped lanthanum chromite perovskites depending upon preparation method and Sr doping, E. Suda, B. Pacaud, T. Seguelong and Y. Takeda, *Solid State Ionics*, 151(2002)335-341.

Life evaluation and improvement of performance of materials in Solid Oxide Fuel Cell

Masatoshi Hattori †
(Department of Chemistry for Materials)

Keywords: SOFC, Monte Calro Simulation, Yttria Stabilized Zirconia, Raman spectra

1. The purpose

Solid oxide fuel cells (SOFCs) have been attracting great attention as a promising new method for electrical power generation. SOFCs can provide high total efficiency when used in a cogeneration system because their high operating temperature such as 1000ºC gives the advantage of producing high-temperature discharge gases. They also promise clean power with little NOx emissions. The basic unit of a cell consists of a three-layer structure: anode, electrolyte, and cathode. It is necessary to achieve not only higher performance but also a more stable cell in order to apply SOFCs for practical use, because SOFCs must operate for tens of thousands of hours to be practical. The aim of this research is life evaluation and improvement of performance of materials in SOFCs.

2. Life evaluation of materials of cathode (fuel electrode)

Life evaluation of Ni-YSZ (Yttria Stabilized Zirconia) used for fuel electrode was examined. Not only aging performance test, but also Monte Calro Simulation (MCS) method was used. Grain growth of Ni is controlled, so that the particle diameter of YSZ remains small. The grain growth ratios of Ni/YSZ predicted by our simulations are in good agreement with experiment. The particle diameter ratio of nickel to YSZ needs to be 3 or greater. This research is applicable to the optimization of porosity and interfaces in other triple phase systems.

3. Life evaluation of materials of electrolyte

The electrical conductivity change with annealing at 1000ºC in the Y_2O_3-ZrO_2 (YSZ) system was examined. Among the sintered samples doped with 8.0mol%Y_2O_3 (8.0YSZ), 8.5mol%Y_2O_3 (8.5YSZ), 9.0mol%Y_2O_3 (9.0YSZ), 9.5mol%Y_2O_3 (9.5YSZ) and 10.0mol%Y_2O_3 (10.0YSZ), 9.5YSZ and 10.0YSZ showed no conductivity decrease even for the annealing period of 1000 h, while 8.0YSZ and 8.5YSZ showed significant decrease with time although the initial conductivities were higher than those of 9.5YSZ and 10.0YSZ. 9.0YSZ showed only slight conductivity decrease. The measurement of Raman spectra demonstrated that the deterioration in conductivity related to the gradual formation of fine tetragonal phase in the cubic phase. Consequently, 9.5YSZ was seemed to be optimum as the electrolyte material of solid oxide fuel cells from the point of stability in high conductivity.

† Chubu Electric Power Company, Inc.

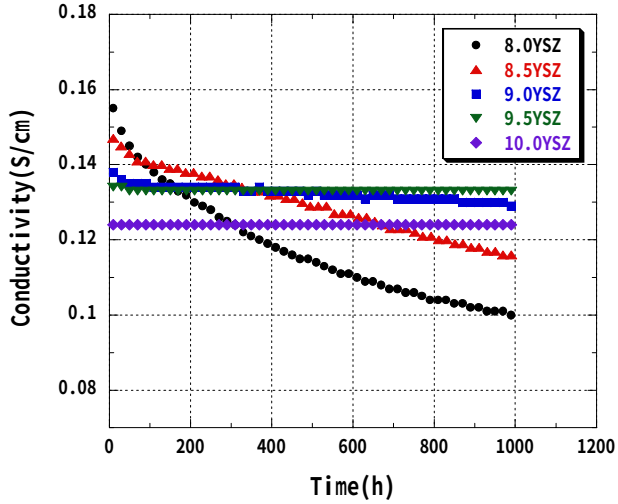

Fig. 1. Time dependence of conductivity of YSZ annealed at 1000℃

4. Improvement performance of electrolyte materials in SOFCs

It is known that Sc_2O_3 doped ZrO_2 with the composition range of X=0.10〜0.12 in $(ZrO_2)_{1.00-x}(Sc_2O_3)_x$ shows the highest conductivity of other ZrO_2-based solid solutions. However, the problem of these solid solutions is the phase transition from rhombohedral to cubic. In this study, the oxide ion conductivity of $(ZrO_2)_{1.00-x}(Sc_2O_3)_{x-y}(Ga_2O_3)_y$(x=0.10〜0.12,Y=0.00〜0.11) were measured.

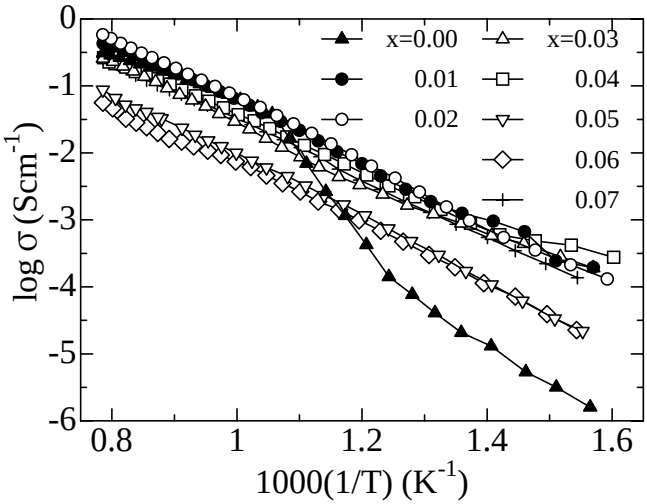

Fig. 2 Arrhenius plots of the electrical conductivity for $(ZrO_2)_{0.89}(Sc_2O_3)_{0.11-x}(Ga_2O_3)_x$

5. Conclusions

In this study, materials of fuel electrode and electrolyte were examined in life evaluation. and high performance materials of electrolyte was examined. The result of this study is expected to be useful on development of SOFCs.

[1] M. Hattori, Y. Takeda, S. Ohara, J.-H. Lee, K. Mukai, T. Fukui, Y. Sakaki and A. Nakanishi, *Change in Conductivity of Yttria Stabilized Zirconia*, Journal of the Japan Society of Powder and Powder Metallurgy, **50**, 297 (2003)

[2] M. Hattori, Y. Takeda, Y. Sakaki, A. Nakanishi, S. Ohara, K. Mukai, J.-H. Lee and T. Fukui, *Effect of aging on conductivity of yttria stabilized zirconia*, Journal of Power Sources, **126**, 23 (2004)

[3] M. Hattori, Y. Takeda, J.-H. Lee, S. Ohara, K. Mukai, T. Fukui, S. Takahashi, Y. Sakaki and A. Nakanishi, *Annealing effect of electrical conductivity in the Y_2O_3-ZrO_2 system*, Journal of Power Sources, in Press

Degradation of Organohalogen Compounds by Using Zero Valent Metals in a Continuous Flow System

Ahmed H. A. Dabwan*

Key words: Degradation, Continuous flow system, Trihalomethanes, Zero valent metals, Bimetals, Ag/Zn bimetal, Passive layer.

1. Introduction

Contamination of underground water is dominated by halogenated organic compounds (HOCs) that represent serious environmental threat due to their toxicity and resistance to natural biodegradation. Significant efforts have been made to develop effective means of eliminating these highly stable compounds from the environment. However in each technique there are limitations and disadvantages.

Treatment of halogenated hydrocarbons by active metals looks promising technique. So far, two means of applying this process have been demonstrated in the field. One involves placing a permeable zone of granular metal across the path of a contaminant plume. Remediation is achieved as the plume flows through the reactive barrier. The other approach involves circulating waste streams or water from pump-and-treat systems through above-ground reactors packed with a mixture of active metal and other materials.

The purpose of this study is to develop a continuous flow system for the degradation of trihalomethanes (THMs) by using zero valent metals. Pure Zn, Ni, and bimetallic Ag/Zn were used to evaluate their capability in degradation. THMs represent the most common disinfection by-product besides their application in many areas. Degradation was carried out under mild conditions in order to reduce the cost and to save energy.

2. Results and discussions

At room temperature however, previous literatures showed that in the Zn/HOCs/H_2O mixture, the influence of oxide film forms immediately in the metal surface is the main obstacle to proceed the reaction even with high amount of Zn^0 powder. In order to overcome this problem, we assumed that working under mild temperature (25-50^oC) would lead to destabilization of the passive layer. Under the experimental conditions complete degradation was achieved for all THMs. Even though complete degradation and high yield efficiency were obtained for both bromoform (BR), and chlorodibromomethane (CDBM), it was noticeable that chloroform (CH) and bromodichloromethane (BDCM) were found to behave different than BR, and CDBM due to the formation of CH_2Cl_2 as intermediate by-products. CH_2Cl_2 is well known persistent compound. The principal products obtained in the continuous flow system when Zn powder was used as an active metal were Cl^-, Br^-, CH_4, C_2H_4, and C_2H_6. Ni powder was used to check its efficiency in the degradation of DBCM, the yield of bromide and

* Division of Material Science (Department of Chemistry for Materials)

chloride ions were relatively low even at high temperature (80^{o}C). In another work degradation of THMs mixture was investigated by using bimetallic Ag/Zn in a batch system in order to obtain more information about the reaction kinetics for each THM. In this experiment, degradation rate follow the order BR>CDBM>BDCM>CH, and the THMs were readily degraded by bimetallic Ag/Zn system. Furthermore, the effect of bimetallic Ag/Zn powder on degradation of THMs mixture in a continuous flow system was also investigated including acid, neutral, and base medium. Precipitation of 3.3% of Ag on the surface of Zn powder caused complete degradation even at room temperature. It seems that rapid oxidation of Zn was prevented due to the presence of Ag on the surface which presumably reduces the activation energy needed to proceed the reaction, and due to the large potential created by coupling active metals as well. The main products were Cl^-, Br^-, CH_4, C_2H_4, and C_2H_6.

Multi-step reduction sequence seems to be reasonable to interpret the mechanism involved in the batch system. Data shows that the disappearance of the primary substrate (THMs) proceeds by kinetics that are first-order. In the reactor the molecule is consumed continually in the axial direction.CHX_3 molecule undergoes hydrogenolysis to give CH_2X_2. Once CH_2X_2 is formed it undergoes further hydrogenolysis to form CH_3X, eventual product of this process is CH_4. The other possible route is the formation of radicals and carbenes that leads to the formation of CH_4, C_2H_4, and C_2H_6. It is well known that Zn serves as the best metal for carbeniod. This idea was supported by the GC-FID data where CH_4, C_2H_4, and C_2H_6 were detected.

3. Conclusion

This system could be generalized to treat not only THMs, but also other halogenated hydrocarbons. The toxicity in these compounds is essentially attributed to the existence of halogen atoms. Detoxification driving force is based on the dissolution of metals flowed by coupled hydrogenation of the carbon-halogen bond which is common in all halogenated hydrocarbons.

Author's publications

1. T. Suzuki, A. H. A. Dabwan, A. Yasue, S. Kaneco, and K. Ohta, Degradation of carbon tetrachloride in a continuous flow system using nickel powder, *ITE Lett. Batt. New Technol. Med.*, **1 (4)**, 617-620 (2000).
2. A. H. A. Dabwan, T. Suzuki, S. Kaneco, H. Katumata, and K. Ohta, Continuous Dechlorination of chloroform of chloroform in a flow system using powder under mild conditions, *ITE Lett. Batt. New Technol. Med.*, **3 (5)**, 585-588 (2002).
3. A. H. A. Dabwan, T. Suzuki, S. Kaneco, H. Katumata, and K. Ohta, Degradation of $CHBrCl_2$ in a continuous flow system using metal powder under mild conditions, *ITE Lett. Batt. New Technol. Med.*, **4 (4)**, 461-464 (2003).
4. A. H. A. Dabwan, T. Suzuki, S. Kaneco, H. Katumata, and K. Ohta, Continuous degradation of chlorodibromomethane in a flow system using zinc powder under mild conditions, Photo/Electrochem. Photobiol. Environ. Energy Fuel, 163-171 (2003).
5. S. Kaneco, H. Watanabe, A. H. A. Dabwan, H. Katumata, T. Suzuki, and K. Ohta, Electrochemical decomposition of bromoform under mild conditions, *ITE Lett. Batt. New Technol. Med.*, **3 (2)**, 201-204 (2002).
6. A. H. A. Dabwan, T. Suzuki, S. Kaneco, H. Katumata, and K. Ohta, Continuous debromination of bromoform in a flow system using zinc powder under mild conditions, Intern. J. Environ. Studies, submitted.
7. A. H. A. Dabwan, T. Suzuki, S. Kaneco, H. Katumata, and K. Ohta, Column degradation of trihalomethanes using bimetallicAg/Zn under mild conditions, Applied Cat. B: Environ., submitted.

Electrothermal atomic absorption spectrometric determination of trace elements in environmental samples with slurry sampling and preconcentration techniques

Md. Nurul Amin†

Key words: Electrothermal atomic absorption spectrometry, Metal tube atomizer, Slurry sampling, preconcentration on tantalum wire

1. Introduction

Environmental analytical chemistry is an important area in environmental chemistry to evaluate the possible health risk and control of environmental exposure of the general population to toxic chemicals. From the viewpoint of environmental risk, environmental samples such as foods, river waters and medicines should be regularly monitored in order to reduce the risks of health hazard. Therefore, it is necessary to develop a rapid, sensitive, simple and low cost method for the determination of trace and toxic element at low levels in the environmental samples. Various atomic spectrometric methods form an essential part of the modern instrumental methods of analysis. Electrothermal atomic absorption spectrometry (ET-AAS) with a metal tube atomizer is shown to provide better sensitivity for most metal elements, and better reproducibility at relatively low power and low cost. In the present study, ET-AAS determination of trace elements in environmental samples was developed in combination with slurry sampling and tantalum wire preconcentration techniques.

2. Experimental

A molybdenum tube atomizer (20 mm x 1.8 mm i.d., wall thickness 0.05 mm), made from purity molybdenum sheet (99.95 % purity, Rembar), was used for slurry sampling ET-AAS for manganese, copper and cadmium analysis. The samples were injected by means of a glass micropipette through a 0.3 mm diameter hole at the mid point of the tube. The atomizer was mounted on two supports so that there was no localized variation in tube temperature. The microtube atomizer was enclosed in a Pyrex chamber (300 mL volume) which had two silica end-windows to allow transmission of the light beam. The chamber was flushed with inert gas to protect the atomizer from oxidation by entrained air. Power for heating the atomizer was supplied by a stepdown transformer. Switching was done with a manual double-pole double-throw switch and timing was done with a stopwatch.

Atomic absorption measurements were performed using a Nippon Jarrell-Ash 0.5 m Ebert-type monochromator equipped with an R928 photomultiplier (Hamamatsu Photonics Co.), a fast response amplifier, a storage oscilloscope (Kenwood CS-8010) and a microcomputer (PC 9801 FA, NEC Corporation). The atomizer was a tungsten tube (20 mm long and 1.5 mm i.d., 0.05 mm thick and 99.95% purity, Rembar Co.). The electric power for heating the atomizer was supplied by two transformers (Yamabishi volt-slider, S-130-30, Cap 3 kVA). Two pinhole apertures were placed in the front and rear of the atomizer, in order to collimate the light beam and eliminate the radiation from the atomizer surface. Tantalum wire for adsorption preconcentration of chromium and antimony were 17 mm long with a diameter of 0.5 mm (99.95% purity, Goodfellow Co.).

† Division of Materials Science (Department of Chemistry for Materials)

3. Results and discussion

Results obtained for the determination of manganese and copper in the three herbal medicine samples and cadmium in Bangladeshi vegetable samples by the proposed method were in good agreement with those measured in the nitric acid digested samples. To validate the precision and accuracy of the method recovery tests were performed, which shows a recovery in the range of 105 to 108%, 89 to 115% and 97 to 103% for manganese, copper and cadmium, respectively. The result of the present study shows that analysis of trace elements in biological samples are shown to be an optimistic by slurry sampling with molybdenum method using ET-AAS. Applications of this recommended technique can be extended to the routine analytical task for other kinds of biological and environmental samples provides good analytical performance with the advantages of simplification of sample pre-treatment, diminishing the turnaround time and operational work, less risks for sample contamination, minimization of analyte losses caused either by the pre-treatment operations or by the incomplete release of the analyte from the solid matrix, it prevents the use of dangerous and corrosive reagents, applicability to both organic and inorganic samples, capability for micro-heterogeneity measurements, faster analytical capability and lower cost.

A direct preconcentration method for ultra trace concentrations of chromium and antimony in river waters adsorption on a tantalum wire followed by electrothermal atomic absorption spectrometry combined with a laboratory constructed tungsten tube atomizer has been developed. Preconcentration has frequently been applied in the determination of ultra trace analytes in complex matrix samples by instrumental analysis. The best pH for the adsorption of chromium and antimony was 3 and 2, respectively. The optimal immersing time was 120 s for both. Under the optimal conditions, the detection limit of chromium and antimony by the tantalum wire preconcentration method was 15 pg/mL and 50 pg/mL (3 S/N), respectively. The relative standard deviation for 5 μg/L of chromium was 9.7% for 10 measurements, while in the case of antimony was 9.4% for 14 measurements. The relatively large RSD may be attributed to the variation in the position with respect to the water surface by stirring. The effects of large amounts of concomitants on the preconcentration of chromium and antimony were evaluated. Even though 10^3-10^4 fold excess of matrix elements existed in water, the chromium and antimony response were not significantly affected by the matrix elements. To validate the precision and accuracy of the method recovery tests were performed, which shows a recovery of spiked-chromium and antimony in the range of 95.8 to 10% with RSD better than 10% for >5 measurements and 99.5 to 114% with 12% for >3 replicate analysis, respectively.

4. Conclusion remarks

The technique developed was shown to be a attractive specific features of ET-AAS are excellent absolute limit of detection, microsampling for slurries, solids and liquids, relatively simple pre-instrumental treatment, reliable contamination control and coupling with enrichment techniques-down to ng/L limit of detection. The proposed method fulfills the requirements of a fast and rugged routine procedure for the reliable determination of trace and toxic elements, with high accuracy, in a wide variety of environmental samples. Thus, the recommended method will be useful for reliable measurement as a regular quality control technique and or as a screening approach in different processes such as industrial and environmental fields.

Author's publications

[1] M.N. Amin, H. Okada, S.I. Itoh, T. Suzuki, S. Kaneco and K. Ohta, Fresenius J. Anal. Chem., **371,** 1130-1133 (2001).
[2] M.N. Amin, S. Kaneco, T. Suzuki, Y. Taniguchi and K. Ohta, Anal. Bioanal. Chem., **373,** 205-208 (2002).
[3] M.N. Amin, S. Kaneco, T. Suzuki and K. Ohta, Microchem. J., **74,** 181-186 (2003).
[4] M.N. Amin, S. Kaneco, K. Nomura, T. Suzuki and K. Ohta, Microchim. Acta, **141,** 87-91 (2003).
[5] M.N. Amin, S. Kaneco, T. Suzuki and K. Ohta, Intern. J. Environ. Anal. Chem., **83,** 1035-1044 (2003).
[6] M.N. Amin, S. Kaneco, T. Suzuki and K. Ohta, Res. Rep. Fac. Eng. Mie Univ., **28,** 9-24 (2003).

A Study on Application of Fractal Analysis to Solve Surface Problems in Manufacturing and Nanofabrication Processes

Mir Behdad Khamesee
(Department of Mechanical Engineering, Division of Materials Science)

Keywords: material testing, measurement, surface nanostructure, nanofractal analysis, nanotechnology, atomic force microscope, two-dimensional fast Fourier transformation, computer simulation, computer-aided engineering

1. Introduction

In metal forming operations, surface structures of metals and tools are closely related to various surface problems, i.e., forming limit, coating feasibility, galling and other tribological characteristics. Recently, the accuracy and quality of nanotechnology processes have markedly improved, and thus, information related to the detailed geometry of such surface structures on the nanometer scale has become necessary as well as their complexities. Although a number of investigations on material surface phenomena have been carried out, as of yet information on surface nanostructures has been insufficient. One of the reasons is that, the surface structures involve various classes of randomness and are difficult to characterize quantitatively. In order to analyse these structures, the authors proposed a fractal approach, and verified its validity against our past researches, where one-dimensional fractal analyses were employed under a micro/meso scale.

The self-affinity and fractal nature property of these surfaces are investigated. Next, the fractal approach is extended to the two-dimensional (2D) fractal method, and thus, the two-dimensional fast Fourier transformation (2D-FFT) analysis is also applied to these surfaces. Moreover, by modeling the 2D power spectrum distribution, a method for simulating the surface nanostructures of any materials is presented, and also its validity is examined for various materials with in-plane isotropic and anisotropic surfaces. In addition, based on these results, a CAE system composed of 2D-FFT and inverse FFT (IFFT) is advanced, and its application is presented and discussed regarding the various surface problems.

2. Power Spectrum Method

The power spectrum S_P and the wavelength λ were obtained by applying one-dimensional FFT analysis to the surface profile curves, and the following relation was assumed.

$$S_P \propto \lambda^{\beta} \quad (1)$$

The fractal dimension D_{PS} was determined from the slope of the log (S_P) vs log (λ) plot, denoted by β, as:

$$\begin{aligned} D_{PS} &= 2, && 0 \leqq \beta < 1 \\ D_{PS} &= E + (3-\beta)/2, && 1 \leqq \beta \leqq 3 \\ D_{PS} &= 1, && 3 < \beta \end{aligned} \quad (2)$$

where E is the Euclidean dimension, and $E = 1$ in this study.

3. Zeroset Method

Intersections of surface irregularities and the basal plane, referred to as zeroset elements here, are generated and their shapes are directly observed. Even if surfaces are self-affined and isotropic in-plane, the resultant zeroset elements become self-similar and reduce their fractal dimensions by one. When the area and the peripheral length of each zeroset element are denoted by Az and Lz, respectively, the fractal dimension Dz is obtained from the following relation.

$$Az^{1/2} \propto Lz^{1/Dz} \quad (3)$$

When the relation between Lz and Az is measured experimentally, the zeroset dimension Dz can be determined by the following equation from the slope of the log(Lz) vs log(Az) plot, denoted by α_Z.

$$Dz = 2\alpha z \quad (4)$$

4. Nanofractal Dimensions

The relationship between the power spectrum S_P and wavelength λ of A1100-O was investigated, where a linear relationship was found between S_P and λ. Moreover the relationship between S_P and λ for all the tested materials was investigated. It was found that relation (1) holds for all materials, showing a fractal nature. The zeroset dimension Dz and the power spectrum dimension D_{PS} have different values. Dz is a direct measure of the complexity of surface irregularities, whereas D_{PS} is different from the physical viewpoint in that it is a measure of wavelength dependability when the surface is viewed as a spectrum. If the magnifying power increases, Dz decreases, indicating that the surface becomes smooth. On the other hand, D_{PS} slowly increases with increasing magnifying power, in contrast to Dz. This shows that the influence of the short-wavelength ingredient of a cross-sectional curve is re-

flected strongly, when the magnifying power increases. According to the self-affinity and two fractal analyses, all the tested surfaces were found to be self-affined fractals in the range down to at least *SR*=500nm, corresponding to a resolution of 1nm.

5. Two-Dimensional FFT Analysis on Material Surface

Employing one method, 2D-FFT was carried out on 2D-AFM images of in-plane anisotropic aluminum sheets (A1100-O), and their power spectra were examined. The spectrum obtained by FFT shows the strength of the power spectrum S_P in each (*kx*,*ky*). The values of *kx* and *ky* are wave numbers of unit of length in the *x* and *y* directions, where *x* corresponds to the rolling direction and *y* is the direction perpendicular to it. The curves were examined using the constant values of *ky*, and the result was the same. Accordingly, it was concluded that the power spectrum image is symmetrical through two midplanes, and thus, the image was divided into four portions (A, B, C, D). Therefore, if the portion of A is modeled, the whole power spectrum image can be determined.

6. Examination on surface smoothing in high-precision metal forming

One of the applications of the present CAE system is to confirm the possibility of its utilization to the nanotechnology process in metal forming. After pressing, the surface roughness *Rz* was measured for each compression ratio e_C in the cases of 0° and 90° directions. The *Rz* decreases with increasing compression ratio, indicating that the plastic deformation causes the large-wavelength components to grow, which reduces the surface complexity. The roughness of the tool surface was 50nm, and the minimum *Rz* in the pressed surfaces was 140nm at a compression ratio of 65%. These simulation results were in good agreement with the experimental results. α which expresses roughness characterizations, decreases with increasing compression ratio, and this tendency is matched with a variation of *Rz*. In addition, the surface complexity which decreases with increasing compression ratio is matched with a change in β. Thus the quality of the deformed surface structure can be judged by these parameters. Therefore, the proposed system is regarded as useful for understanding the surface nanostructures of products manufactured through high-precision press forming. Finally, while the 3D surface information constitutes 512×512 elements, it can be reproduced through only three parameters α, β and γ using the advanced CAE system. Accordingly, the system is also regarded as applicable to so-called information compression.

7. Concluding Remarks

The results obtained in the present research are summarized as follows:

1) From the results of the one-dimensional fractal analysis, it was found that the surfaces of all used materials are self-affined fractals at a resolution of 1nm.

2) The results obtained for two-dimensional FFT of AFM images showed that the meridian cross-sectional curve had a fractal nature.

3) The spectrum distribution could be modeled adequately by introducing its symmetry in the wave-number space and an anisotropic parameter.

4) By using only three parameters a simulator was successfully developed, which can carry out the creation of three-dimensional surface features at the same level of complexity as that of the actual surface.

5) A CAE system composed of 2D-FFT and 2D-IFFT was constructed for quantitative estimation of the surface structures and its various applications were shown to be valid.

6) The mass data of surfaces could be compressed into only three parameters using this system. This compressed information includes all surface waviness, complexity, irregularity, roughness and anisotropic properties.

Author's Publications

1. M.B. Khamesee, Y. Kurosaki, M. Matsui and K. Murai, "Nanofractal Analysis of Material Surfaces Using Atomic Force Microscopy", Materials Transactions, Journal of the Japan Society for Technology of Plasticity, Vol. 45, No. 2, February 2004, pp. 469-478.
2. M.B. Khamesee, M. Matsui, K. Murai, T. Ishihara and Y. Kurosaki, "Quantitative Estimation of Fracture Surface for Mild Steel Using Fractal Analysis", Proceedings of the 6th International Symposium on Microstructures and Mechanical Properties of New Engineering Materials (IMMM), Wuhan, China, October 2003, pp. 147-152.
3. M. Matsui, Y. Kurosaki, M.B. Khamesee and K. Murai, "Prediction of Free Surface Profile of Sheet-Formed Products Using a Fractal Approach", Journal of the Japan Society for Technology of Plasticity (JSTP), Vol. 43, No. 498, July 2002, pp. 644-648.
4. M.B. Khamesee, Y. Kurosaki, M. Matsui and K. Murai, "Fractal Approach for Prediction of Surface Profiles of Sheet-Formed Products", Proceedings of the 4th International Conference on Mechanics and Materials in Design (MMD-4), Nagoya, Japan, June 2002, pp. 175-176.
5. M. Matsui, Y. Kurosaki, M.B. Khamesee and K. Murai, "A Study on Predicting the Surface of Pressed-Products Using Fractal Analysis", Proceedings of the 51st Conference of the Japan Society for Technology of Plasticity (JSTP), Seki, Japan, November 2000, pp. 455-456 (in Japanese).
6. Y. Kurosaki, M. Matsui, K. Murai, T. Ishihara, M.B. Khamesee and Y. Tamaki, "A Study on the Quantitative Estimation of the Fracture Surfaces for Analysis of Accidents", Proceedings of the 51st Conference of the Japan Society for Technology of Plasticity (JSTP), Seki, Japan, November 2000, pp. 333-334 (in Japanese).

Degradation of endocrine disrupting chemicals in environmental samples by microorganisms and application to their easy analysis

Aleya Begum†

Keywords: Phthalic acid esters, *Saccharomyces cerevisiae*, *Bacillus subtilis*, metabolites, degradation pathway, preconcentration, immobilized.

1. Introduction

Phthalic acid esters (PAEs), which are widely used as plasticizers and are produced in large quantities, have received extensive attention in recent years due to their widespread use and ubiquity in the environment. Degradation based on the activity of enzymes and microorganisms, such as bacteria, fungi, algae and protozoa, are of growing importance for degradation and sorption of chemical compounds, due to their simplicity, rapidity, cost-effectiveness and reproducibility. Microorganisms immobilized on several inorganic adsorbents have been used for preconcentration and speciation of trace metal ion.

2. Experimental

PAEs were dissolved in Ammonium di-hydrogen phosphate (ADP) solution (cultivation medium). Yeasts were grown in the cultivation medium at 40 °C for 15-60 min. The cultivation was performed at 20-50 °C for 12-72h. After the cultivation, the PAEs solution with yeasts were filtered through a membrane filter (0.5 μm). The filtrate used for PAEs analysis.The PAEs concentrations of all samples were determined by high performance liquid chromatography (JASCO Co., Tokyo, Japan) with a UV detector (254 nm). The intermediate products were analyzed by gas chromatography-mass spectrometry (GC/MS) using a Model QP5000 (Shimadzu Co., Kyoto, Japan).

For adsorption *Saccharomyces cerevisiae* was grown in 20 mL of sample solution containing ADP at 40 °C for the growth of yeast. The cultivation was performed at 20–50. After cultivation, the solutions were filtered and the filtrate used for PAEs analysis.

For the immobilization of yeast cells, dry yeast was mixed with silica gel at 1:5 ratio. The mixture was wetted and mixed with water, then the paste was heated in an oven at 105°C for 3 h to dry the mixture. A glass column plugged with a small portion of a glass wool was filled with *S. cerevisiae* immobilized on silica gel. The PAEs solutions were separately passed through the column at a flow rate of 3 mL min^{-1}. Then, the retained PAEs were eluted from *S. cerevisiae* immobilized on silica gel with 2.5–7.5 mL ethanol. The analytes in the eluates obtained were determined by HPLC.

For the preconcentration of trace silver, yeast with $(NH_4)_2HPO_4$, was added to a river water and cultivated at 25 ^{0}C for 2 h. The cultivated mixture was filtered with 3.0 μm membrane filter and the collected yeast on the filter washed with flush ultra-pure water and 0.1 *M* nitric acid. Atomic absorption measurements were made with a Nippon Jarrell-Ash AA/AE spectrophotometer (AA-855) equipped with an auto-background corrector and a graphite furnace atomizer (Tube type 228-3110).

† Division of Materials Science (Department of Chemistry for Materials)

3. Results and discussion

A degradation process of endocrine disrupting chemicals such as phthalic acid esters (PAEs) by microorganism has been developed. The biodegradation of phthalic acid esters namely, Diethyl phthalate (DEP), Dibutyl phthalate (DBP) and Butyl benzyl phthalate (BBP), in aqueous solutions with baker's yeast *S. cerevisiae* and DBP with *Bacillus subtilis* (formerly *Bacillus natto*) were investigated. Ammonium dihydrogen phosphate(ADP) was used as a culture medium. Under optimum conditions the degradation rate of DEP, DBP, and BBP were 62%, 96% and 90% respectively by *S. cerevisiae* The kinetics study demonstrated that the biodegradation of DEP, DBP and BBP by *S. cerevisiae* conformed to the first-order reaction. In the case of *B. subtilis*, under the optimal conditions, the degradation percentage of DBP was 72% after 24 h cultivation.

The metabolites of DEP appeared to be ethyl methyl phthalate (EMP), dimethyl phthalate (DMP) and phthalic acid (PA), whereas dipropyl phthalate (DPP), diethyl phthalate (DEP), monobutyl phthalate (MBP) and PA were identified as metabolites of DBP, and MBP, DEP and PA were appeared as metabolites of BBP. In the case of *Bacillus subtilis*, the metabolites of DBP were identified as DPP, MBP and PA.

The adsorption behavior of DEP and DBP from aqueous solution to baker's yeast was quantitatively characterized. The experimental results showed that the adsorption efficiency of DBP was much higher than that of DEP. The heat of adsorption of DBP was 373 KJ mol^{-1}, indicating that the adsorption behavior seemed to be chemical adsorption.

The PAEs were preconcentrated on *Saccharomyces cerevisiae* immobilized on silica gel Several parameters on the recovery of the analytes were investigated. Recoveries of BBP, DBP and DCHP were 100±2, 98±2 and 98±3%, respectively, at 95 % confidence level under optimum conditions. The capacity of the adsorbent was found to be 1 .4 mg g^{-1} for BBP and DBP, and 3.6 mg g^{-1} for DCHP. The proposed method was successfully applied to the determination of PAEs in river water with high precision and accuracy.

A new preconcentration method with baker's yeast was evaluated for the determination of trace silver in river waters by graphite furnace atomic absorption spectrometry (GFAAS). Under optimal conditions, silver in aqueous sample was concentrated to 6.9-fold by yeast. The recovery of spiked silver was in the range of 89 to 110%. By the preconcentration, it was found that ultra trace silver in river waters could be determined without interferences of matrix elements, after only the cultivation and with no chemical treatment.

4. Conclusion

The proposed biodegradation and biosorption method by microorganisms offer great promise for the accelerated, very simple, inexpensive, and safe removal and cleanup of organic and inorganic pollutants from the environment. Thus, the yeasts will be a suitable candidate for endocrine disrupting chemicals degrade and removal from environmental contamination site.

Author's publications

[1] K. Ohta, K. Saruma, S. Kaneco, T. Suzuki, S. Itoh and A. Begum, *Annali. di. Chim*., **92,** 587-594 (2002).
[2] A. Begum, H. Katsumata, S. Kaneco, T. Suzuki and K. Ohta, *Bull. Environ. Contam. Toxicol,*, **70,** 255-261 (2003).
[3] A. Begum, H. Katsumata, N. Sakuma, S. Kaneco, T. Suzuki and K. Ohta, *Photo/Electrochem. Photobiol. Environ. Energy Fuel*, 155-162 (2003).
[4] A. Begum, H. Katsumata, S. Kaneco, T. Suzuki and K. Ohta, *Fresenius Environ. Bull.*, **12,** 1309-1314 (2003).
[5] H. Katsumata, A. Begum, S. Kaneco, T. Suzuki and K. Ohta, *Anal. Chim. Acta.*, **502,** 167-172 (2004).
[6] A. Begum, H. Katsumata, S. Kaneco, T. Suzuki and K. Ohta, *Environ. Eng. Sci.*, submitted.
[7] A. Begum, H. Katsumata, S. Kaneco, T. Suzuki and K. Ohta, *J. Environ. Management,* submitted.

Mechanistic Study for Efficient Photo-initiator Generation

Koichi Kawamura †

Keywords: Polymerization, Photoinitiation, Radical, Sensitization, Merocyanine, Electron transfer

1. Introduction

Many attempts have been made to develop efficient photoinitiating polymerization systems that can be used upon visible light excitation since such systems are expected to have wide applications in typical practical fields, such as high-speed photopolymers in computer-to-plate laser imaging and 3D polymerization systems. In such systems, the photopolymerization occurs by electron transfer from a photo-excited donor (dye) to an acceptor (initiating part) molecule. It is generally accepted that the rate of the electron transfer K_{et} depends not only on the free energy change but also on the distance between donor and acceptor. Dye-linked photoinitiators, in which a radical generating part is brought close to a photosensitizing dye-chromophore by a covalent bond, have been shown to be very useful as free-radical sources. However, the details of photo-processes of those systems are not clear. In order to investigate these issues, we have prepared several dye-linked photoinitiating systems and investigated their photochemical behaviors. For this purpose, the following new photoinitiators (Figure 1) were prepared, in which a merocyanine chromophore and a bis(trichloromethyl)-1,3,5-triazine chromophore were linked by a different number of methylene chains (MT1, MT3) and at different positions (MT1, MT2).

2. Results and Discussion

The absorption spectra of linked compounds (MT1, MT2 and MT3) were almost identical with that of an equimolar mixture of each component merocyanine and triazine (M+T). This indicates that there is no appreciable interaction between these two chromophores in the ground state. The spectral change observed by steady-light irradiation of MT1 in deaerated toluene are shown in Figure 2. When a solution of MT1 was irradiated with a light of 430 nm wavelength, where only the dye was excited, the band at 430 nm that is characteristic of the dye disappeared and a new band showing its maximum at 380nm appeared, with an isosbestic point at 390 nm. Similar spectral changes were observed under irradiation of other MT systems.

In marked contrast, similar irradiation of an equimolar mixture of the dye (M) and the triazine (T) showed essentially no change at least in the time range where appreciable decay was noted for the linked system. The observations can be interpreted as indicating that MT systems undergo intramolecular electron transfer reaction upon photoexcitation much faster than M+T system under these conditions.

The relative efficiency of merocyanine-linked triazines as an initiator in photoinitiating systems of acrylates monomers was evaluated by monitoring the disappearance of the acrylic double bond in the IR absorption (Figure 3). Three merocyanine-linked photoinitiators, MT1, MT2, and MT3 and physical mixtures of merocyanine/triazine were used. The results clearly showed that the rate is markedly enhanced when the linked photoinitiators were used, as opposed to the unlinked photoinitiator combinations. Among the liked initiators, MT3 is much less effective for photoinitiating polymerization than MT1 and MT2, and MT2 shows

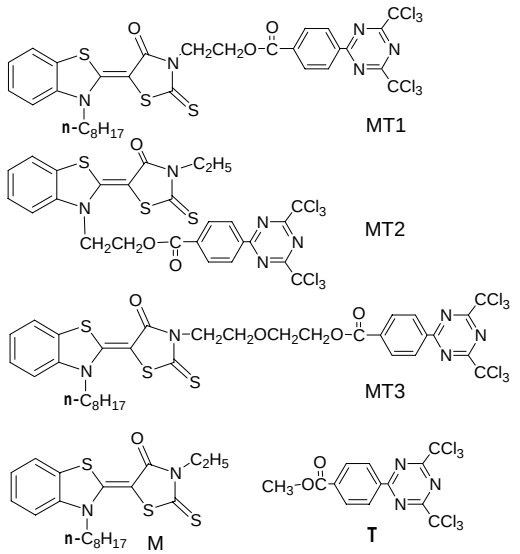

Figure 1. Dye-linked initiators (MT1, MT2 and MT3) and reference compounds (M, T).

† Fuji Photo Film Co., Ltd.,

larger initiation rate than MT1, although they have the same number of methylene chain.

The major difference between MT1 and MT2 is the position to which the triazine is connected to the dye. The reason for the enhanced interaction in MT2 may be attributable to the more effective orbital interaction between the triazine moiety and the photoexcited sensitizing moiety in MT2 system, compared to that in MT1 system. We evaluated the donor-acceptor distance of the linked compound from the most stable conformer which was obtained by searching low-energy conformations by CONFLEX method in CaChe® calculating system and the result indicates the more effective interaction in MT2 than in MT1.

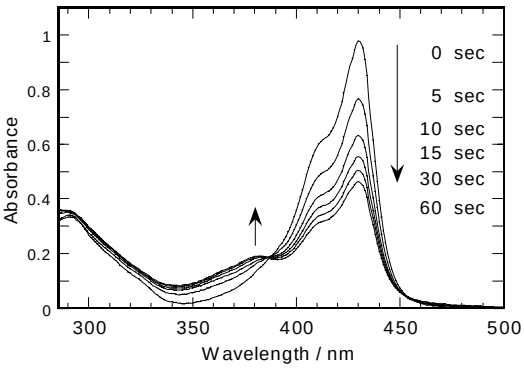

Figure 2. Change of absorption spectra of MT1 upon irradiation at 430nm in toluene.

3. Conclusions

The photochemical and photophysical processes were examined in a solution and in a photopolymer matrix used in practical photopolymerization systems. The initial reaction step between the photoexcited merocyanine and the triazine was concluded to be electron transfer based on the products analysis and thermodynamic considerations. In the dye-linked photoinitiating systems, the number of methylene unit between the light-absorbing moiety and the radical-generating moiety is demonstrated to be an important factor to control the photochemical reactivity. The linking position is also found to show a slight but distinct effect on the efficiency. Those findings give a clue to develop new dye-linked photoinitiators which are highly sensitive to a visible light.

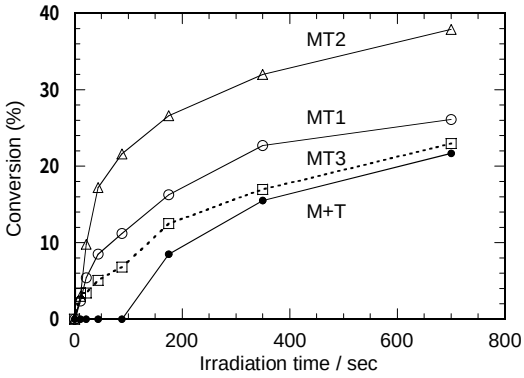

Figure 3. Conversion (%) of acrylate double bonds as a function of time for polymerization of acrylates containing photoinitiators on irradiation (λ= 430 nm, Intensity = 34 mW/cm^2). Photoinitiating system (24mmole/ dm^3) ; M+T (●), MT1 (○), MT2 (△), and MT3 (□).

Author's publications

[1] Koichi Kawamura, Yoshimasa Aotani and Hideo Tomioka, "Photoinduced Intramolecular Electron Transfer between Carbazole and Bis(trichloromethyl)- s-triazine Generating Radicals", *Journal of Physical Chemistry, B,* (2003), **107**, 4579–4586.

[2] Koichi Kawamura, "Novel and Efficient Dye-Linked Radical Generators for Visible Light Photoinitiating Polymerization", *Journal of Photochemistry and Photobiology A: Chemistry,* (2004) **162**, 329–338.

[3] Koichi Kawamura and Kunimasa Kato, "Synthesis and Evaluation as a Visible-Light Polymerization Photoinitiator of a New Dye-Linked Bis(trichloromethyl)-1,3,5-triazine", *Polymers for Advanced Technologies,* (2004) in press.

[4] Koichi Kawamura, "Merocyanine-dye-sensitized Photoinitiator Generating a Free-radical via an Intramolecular Electron-transfer Process", *Chemistry Letters*, (2003) **32**, 1068-1069.

[5] Koichi Kawamura, "Mechanistic Studies of the Photo-decomposition of Substituted Bis(trichloromethyl)- 1,3,5-triazine Sensitized by Merocyanine Dye", *Chemistry Letters* (2003) **32**, 832–833.

[6] Koichi Kawamura, Kunihiko Kodama, Katsuyuki Hirai and Hideo Tomioka, "Laser Flash Photolysis Study of Dialkylphenacyl Sulfonium Salts", *Chemistry Letters*, (2004) **33**, 148–149.

[7] Koichi Kawamura and Fumihiko Sasaki, "Photoinduced Generation of Sulfonic acid from N-Sulfony-Arysulfonamide", *Journal of Photopolymer Science and Technology*, (2001) **14**, 265–271.

[8] Koichi Kawamura, "Intramolecular Electron Transfer in Carbazole Linked Radical Generators", *RadTec Asia '03, Conference Proceedings,* (2003) 185-188.

[9] Koichi Kawamura, "Dye-Linked Photoinitiators; Synthesis and their Characterization", *RadTec Asia '97, Conference Proceedings,* (1997) 271-274.

[10] Koichi Kawamura and Hirotaka Mastumoto, "Dye-Linked Photoinitiators", *Proceedings of 45th Annua1 Conference of the Society for Imaging Science and Techno1ogy* VA, Springfield, (1992) 337-340.

A Study on Distortional Buckling of Thin-walled Light Gauge Steel Members

Koji Hanya*

Keywords: cold-formed steel members, flexural strength, Compression strength, fire resistance tests, strength evaluation methods

Introduction

Cold-formed thin-walled steel members with thicknesses of around 1mm are relatively new structural members in Japan. It is because such a thin steel member had not been long allowed to use as a structural member under the Japanese Building Standard Law. This situation has been changed in recent years through the development of steel-framed houses. Although the use of such a thin steel member is currently possible, there are still some design issues to be clarified for realizing the broader applications, mainly related to its complex buckling behavior. The complex buckling is called distortional buckling (Table 1(b), Table 2 (c)). To study the behavior of this distortional buckling in detail, it was done four kind of investigations in this research.

Table 1 Distortional Buckling of Members

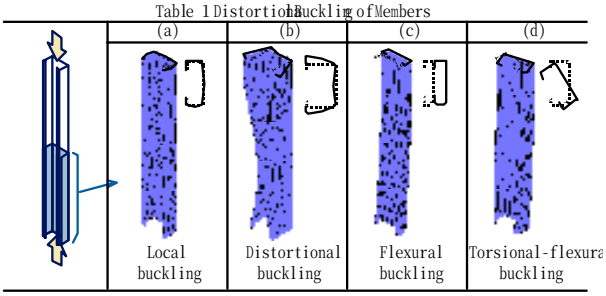

Table 2 Distortional Buckling of Plates

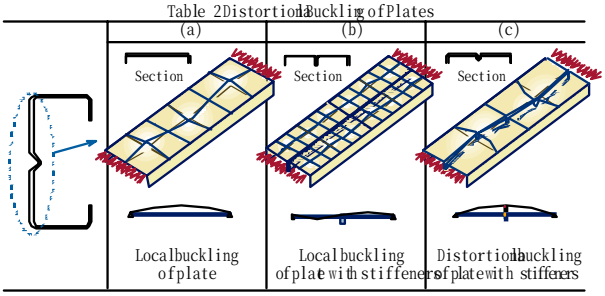

Discussions

1) In the case of flexural members, the distortional buckling is often seen in the floor and roof panels in steel-framed houses. Negative bending tests were therefore conducted for panels consisting of two lipped-channels and structural plywood fastened together with screws (Fig. 1). Twelve bending tests provided detailed behavioral information on distortional buckling and the possible strength evaluation methods for improving the design of thin-walled steel members.

2) In the case of compression members, the panels mainly consist of witch both side of lipped-channels are attached to structural plywood. In this case, the distortional buckling aren't side as the floor and roof panels. Therefore it was conducted first that twenty compression tests of lipped-channels without structural plywood (Fig. 2), and then done the fourteen panels with structural plywood.

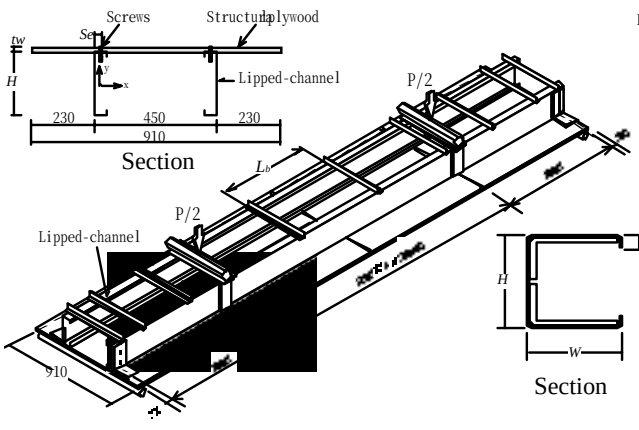

Fig.1 Specimen of Bending Tests

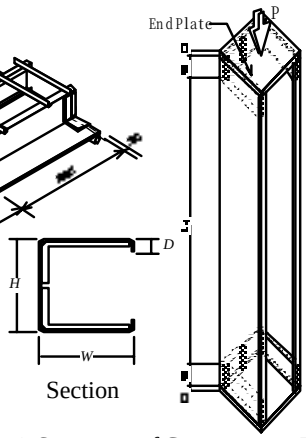

Fig.2 Specimen of Compression Tests

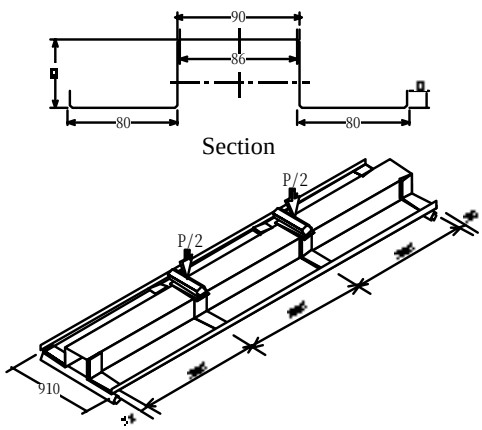

Fig.3 Hat-shaped Specimen

*Nippon Steel Corporation

3) Due to design thin-walled steel members effectively, it is necessary to consider the intermediate stiffeners. It was conducted that eighteen bending tests of hat-shaped sections (Fig. 3), to clarify the relationship buckling behavior and variety of the stiffeners, that is, width, depth, shape and numbers of the stiffeners.
4) The application of the thin-walled steel members to the houses requiring fire resistance has been limited, due mainly to a lack of information on mechanical properties and buckling behavior of such a thin steel member under elevated temperatures. Therefore, material tensile tests and compression column tests were conducted to clarify the characteristics and to examine if information under normal temperature can be applicable. The tests covered a thickness from 0.5mm to 1.6mm and a temperature up to 600ºC.

Conclusions

i) Two types of distortional bucking modes were observed in the tests, the lip-flange distortional buckling and flange-lip distortional buckling with the lipped-channels.
ii) It was able to evaluate the buckling modes with lipped-channels by using an eigenvalue analysis of elastic buckling.
iii) Using the von Karman's formula, it was able to convert the elastic distortional buckling strength into the allowable strength or the effective width, in which the yield point and the post buckling behavior were considered.
iv) It was tried to clarify the relation between the elastic distortional buckling strength and the dimensions of the lipped-channels. From the experimental and analytical investigations, that relationship was given as the simple formulae consisting of height of the web H, width of the flange W, depth of the lip D, thickness of the material t and the buckling length L_b of the lipped-channels.
v) Buckling design formulae for normal temperature may be applied to estimate the column strength of thin-walled steel members under high temperatures up to 600ºC.

Author's publications

[1] Koji Hanya, Ryoichi Kanno, Shosuke Morino : Distortional Buckling of Thin-walled Lipped Channel Partially Restrained with Attached Theathing Subjected to Bending, Journal of Structural and Construction Engineering, No. 567, pp.157-164, 2003.5 (in Japanese)
[2] Shosuke Morino, Jun Kawaguchi, Yasumori Mizuno, Koji Hanya : Distortional Buckling of Light-Gauge Lipped Channel Short Columns, International Journal of Steel Structure Vol. 3, No. 3, pp.203-217, 2003.9
[3] Koji Hanya, Rhoichi Kanno : Study on Composite Panels Consisting of Cold-formed Steel Channels and Plywood with Self-drilling Screws, ASCE Proceedings of Structural Congress XV Vol.1, pp.428-432, 1997.4
[4] Koji Hanya, Ryoichi Kanno, Shosuke Morino,Mamoru Kohno : Material Properties and Buckling Behavior of Cold-formed Thin-walled Steel Members under Flevated Temperatures due to Fire, Journal of Structurak and Construction Engineering No. 582, 2004.8 (in Japanese)

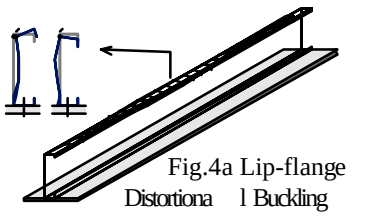

Fig.4a Lip-flange Distortiona l Buckling

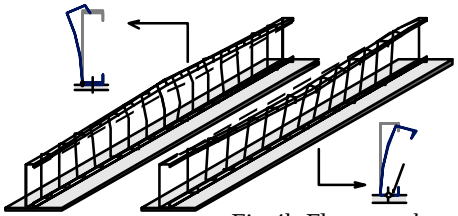

Fig.4b Flange-web Distortiona l Buckling

Fig.5 Distortional Buckling

Fig.6a Local Buckling

Fig.6b Distortional Buckling

Fig.6c Distortional Buckling with Local Buckling

Experimental Studies on Atmospheric Boundary Layer on Complex Terrain and Mutual Interference of Wind Turbines in Large Scale Wind Farm

Takeshi Yokota†
(Department of Mechanical Engineering)

Keywords: wind energy assessment, atmospheric boundary layer, complex terrain, Doppler Sodar, mutual interference, wind tunnel tests

Abstract

Recently, Wind energy penetration is soaring all over the world especially in the European countries, due to the Global Warming Concerns. Also in Japan, several 10MW-Class Wind Farms have appeared in a recent few years, as the results of the new energy promotion programs, which includes the wind energy, by the governmental bodies and the utility companies.

In Japan, the wind resource assessment, for developing the large scale wind farm with several tens of the wind turbines, implies at least two major problems which must be overcome, due to the complexity of topography. The first one is the understanding of the wind profile as a result of the flow distortion due to the complex terrain; the second one is to know how the terrain complexity affects the mutual interference of Wind turbines.

This dissertation settles the all outcomes through the following studies which give the ideas for making solutions of the two major problems as mentioned above. It deserves to be referred both for practical use and academic knowledge.

Chapter 1; Introduction

In this chapter, the state-of-the-art technologies, which contribute the world wide promotion of the wind power generation, are summarized first. Then, after reviewing the investigation history of the wind resource assessment and the mutual interference of Wind Turbines from the literature, these problems in the complex terrain and the objects of this study are pointed out.

Chapter 2; Experimental apparatus and the principle of Doppler Sodar observation.

In order to know the vertical wind profiles in the various topography, this study were carried out by observing it directly from the ground level through 1,000m height with the use of Doppler Sodar. For observing the wind profile, the monostatic method, which is transmitting the tone burst to three directions in the atmosphere by time sharing from one point on a ground, is applied. The principle of acoustic sounding is on the detection of the backscattered signal from refractive index discontinuities or disturbances in the atmosphere. This system is composed of one vertical antenna and two tilted antennas with elevation angle of 70 degree. The tilted antennas are set in the direction of 90 degree each other. The vertical and tilted beams were cycled through three beams once every 10 seconds, that is, one complete data set is obtained once every 30 seconds. Analyzing a set of data, three components of wind velocity and the standard deviation of each component are calculated. The cup anemometers and wind vanes are also used for observing the wind profile in the lower height (10m～20m).

Chapter 3; Assessment of Local Wind Energy by Sodar Technique

This chapter describes the measurement of the atmospheric boundary layer for siting the wind farms. The measurements were carried out at the sea coast at Konbumori cape in Hokkaido Island. The vertical wind speed distributions up to 1000 meters high were measured by means of the Doppler SODAR. The measured wind speed distributions indicate the effects of the geometrical shape and the roughness of the ground depending on the wind direction. Measured wind

† Electric Power Development Co., Ltd.

profile did not agree with power law plots at higher layer. The Weibull distribution also depends on the wind direction and height.

Chapter 4; Measurement of Atmospheric Boundary Layer for Siting Wind Farms.

This chapter describes the measurement of the atmospheric boundary layer for siting the wind farms. The measurements were carried out at the gentle hill at Tomamae town in Hokkaido Island. The vertical velocity distributions up to 1000 meters high were measured by means of the Doppler Sodar. The measured velocity distributions indicate the effects of the geometrical shape and the roughness of the ground depending on the wind direction. The stream wise velocity along the flat ground is decreasing with increasing the distance from sea coastline.

Chapter 5; Wind Power Prediction on Complex Terrain in Japan.

In order to accurate estimation of the future wind energy capture, the vertical and horizontal wind velocity distributions on the complex terrain are measured with the use of Doppler SODAR and meteorological anemometers. The wind velocity reduction due to ground skin friction or ground shape is also shown. Compared to estimation by power law of the wind profile, the estimated power due to the logarithmic law of the wind profile gives better agreement with the actual generation power. The factor of the differences between estimation and measurement is caused by the fluctuation of the wind speed.

Chapter 6; The Wind Assessments and The Power Prediction of Wind Farm in Japan.

In this chapter, the wind assessment for wind farm project in Japan is explained with instance of Tomamae town's wind farm. The wind speed measurement is usually done by using a cup anemometer on the top of a mast (15-20m). In general, the height of the anemometer is lower than the expected hub height of wind turbine to be used. In this study, the Doppler sonic radar is also used for measuring the wind speed at hub height and above. The methods of prediction based on two different experimental methods are discussed. The actual power output of wind turbine is compared with prediction results. The comparison between the low layer measurements (10,15m) and higher layer measurements (0-1000m) are discussed. The vertical velocity distributions have effect on the geographical shape and the surface roughness.

Chapter 7; Experimental Study for Mutual Interference between Two Horizontal Axial Wind Turbines. (In Case of Wind Tunnel Tests for Two kinds of Artificially Generated Flow Patterns)

In order to obtain the fundamental knowledge of turbulence and boundary layer profiles on wake interaction of HAWT's, extensive experiments were performed in a wind tunnel, considering two different flow patterns. This chapter, through wind tunnel testing for two kinds of artificially generated flow patterns, investigates the interaction between two HAWT's and outlines the following points; (1)experimental analysis of wake behind HAWT for two different flow patterns; (2) relationships between HAWT performances and two different flow patterns; (3)detailed investigation for mutual interference between two HAWT's. As the results, (1) The power co-efficient is not strongly affected by the flow turbulence. (2) The wake region of the upper HAW's is spread along the stream. (3) The velocity recovery ratio is bigger when the turbulence intensity of the natural flow is higher. (4) The velocity distribution in the potential core region in the wake of the HAW's is extremely complicated, but in the well developed region, it becomes similar profile. Note that spreading ratio depends strongly on the turbulence of the surrounding flow.

Chapter 8; Conclusion

The overall results and conclusion are summarized in this chapter.

Master-Slave System Characterized by Hybrid Kinesthetic Sense Presentation of Real and Virtual Force

Naoaki Tsuda
(Division of System Engineering)

Keywords: Master-Slave System, Hybrid Kinesthetic Sense, Force Feedback, Virtual Force, Environmental Reflection

Abstract

To attain comfortable maneuverability with master-slave systems, force feedback systems have been studied in various ways. However, no reflective force is returned to the operators when the slave robot works in free space, and doesn't have any contacts with the objects, in this case.

We sometimes intend the slave robot to be in or to come into favorite regions, and/or intend the robot not to enter dangerous regions. It is necessary to notify the operator of the slave robot's situation to meet the operator's intention.

To make the notification more effective, the authors proposed a method to present the kinesthetic sense as a hybrid of a contact-caused real force and a virtual force. The virtual force reflects the slave robot's situation such as position and velocity, and the reflection helps the operator to maneuver the slave robot in the environment with the favorite and/or dangerous regions.

This thesis presents a design method of the proposed system, and confirms the effectiveness of the system through tele-operating experiments.

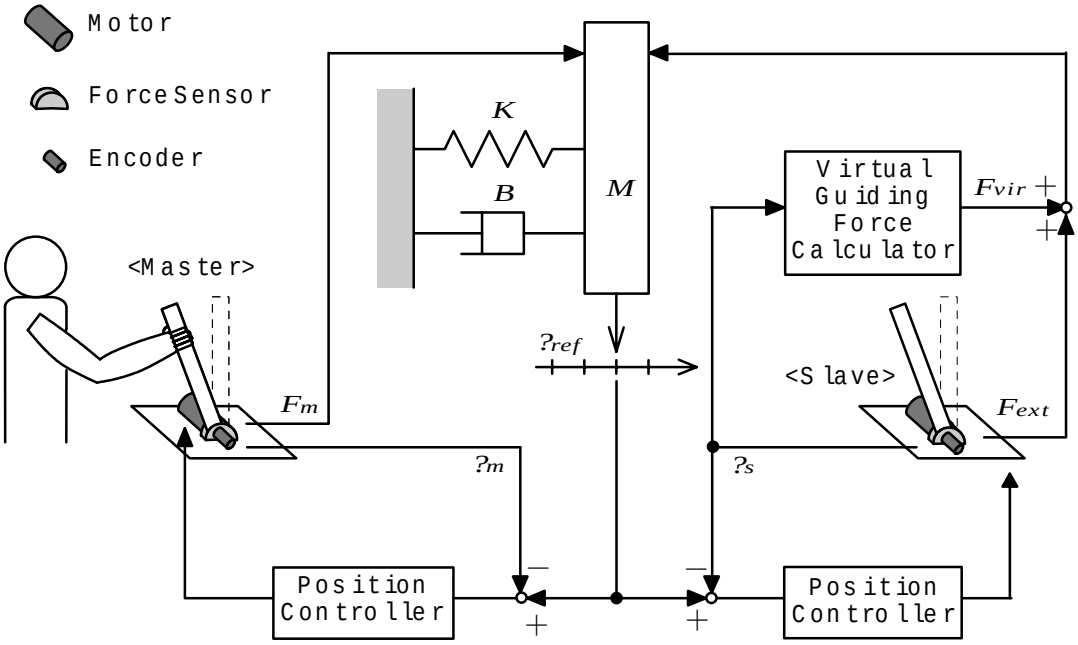

Fig. Master-Slave System Characterized by Hybrid Kinesthetic Sense Presentation of Real and Virtual Force

Construction

In chapter 2, both the conventional force-feedback master slave system and the proposed system that has virtual force feedback are explained.

In chapter 3, equipment that is used in this research is explained.

In chapter 4, an experiment is carried out. In the experiment, the proposed system is applied on the driving system of a car, and the effectiveness of the system is confirmed.

In chapter 5, some experiment are carried out in order to confirm the effectiveness of virtual force feedback.

In chapter 6, designing method of the master-slave system is proposed considering the system's stability. By using this method, several parameters can be tuned easily. The effectiveness is confirmed through positioning experiment.

In chapter 7, a case when the slave robot system is influenced by a disturbance is focused on. There, a disturbance observer is introduced. The effectiveness is confirmed through positioning experiment.

In chapter 8, this thesis is concluded.

Author's publications

[1]N.Tsuda, N.Kato, Y.Nomura and H.Matsui, "Master-Slave System Characterized by Hybrid Kinesthetic Sense Presentation of Real and Virtual Force", Journal of the Human Interface Society, Vol.6, No.1, 2004.

[2]N.Tsuda, N.Kato, Y.Nomura and H.Matsui, "Development of Master-Slave System for Magnetic Levitation", Proceedings of the International Conference on Machine Automation(ICMA) 2000, pp.69-74, 2000, Osaka, Japan.

[3]N.Tsuda, N.Kato, Y.Nomura and H.Matsui, "Design framework of teleoperating system for magnetically levitated robot with force-feedback", Proceedings of SPIE (Telemanipulator and Telepresence Technologies VIII), Vol.4570, pp.25-33, 2002, Boston, U.S.A..

[4]N.Tsuda, N.Kato, Y.Nomura and H.Matsui, "Improvement of Virtual Force-Feedback Teleoperating System Considering a Disturbance", Proceedings of the 3rd China-Japan Symposium on Mechatronics(CJSM2002), pp.167-172, 2002, Chengdu, China.

Study on computer-supported system for mass classes

Naoki Morita
(Aducational Technology, Division of Systems Engineering)

Keyword: Degree of Understanding, Description Answer, e-learning, Natural Language Processing

1. Introduction

It is important for students to ask about the issues that they do not comprehend in lectures. Nevertheless, most students in Japan seldom do so. It makes teachers hard to know whether students comprehend or not (see Kita, et al. 2001.)

To grasp students' comprehension, teachers often give short tests in lectures. In short tests, the use of description-answer style brings better grasp than that of multiple-choice answer style. Because, students must describe their answers with their own words. However, in a large class, it is hard for the teacher to check all description-answers during the lecture. As a result, they cannot give appropriate advices and improve students' comprehension immediately.

2. Idea

If teachers could grasp students' comprehension (even though roughly,) they could immediately modify the lectures according to it.

We propose a real-time description-answer short test system to grasp their comprehension in a large class. The system classifies students' description-answers into several groups of similar contents, since it is easier for teachers to check all classified answers than to do all unclassified ones.

To grasp students' comprehension, teachers need to know major patterns of the answers. In this paper, we assume that similar answers include same keywords. The system divides answers exclusively using the keywords contained in a lot of answers.

3. The method of classifying answers

Based on this idea, the system classifies answers as the following procedure. First, the system extracts candidates of keywords from the answers. Next, it chooses keywords from the candidates and classifies the answers according to the keywords. After that, teachers modify groups appropriately. The details of each process are described as follows.

- Extracting candidates of keywords

Since words in Japanese sentences are not separated by spaces, using the Japanese morphological analyzer "Chasen" (see Matsumoto, 2000,) the system extracts words from the answers and makes them candidates of keywords.

- Classifying answers into groups

The system calculates the weight of each candidate according to its frequency in the unclassified answers. It chooses the candidate with the heaviest weight as the keyword. It gathers all unclassified answers including the keyword into a group. By repeating this process, most answers are classified into several major patterns.

We provide two manual operations to modify groups appropriately.

- Adjusting the weight of each candidate

The system sometimes may not choose keywords that teachers expect. We provide a manual operation that teachers are able to adjust the weight of candidates. Increasing the weight of a candidate enhances the possibility of choosing the candidate as a keyword. Decreasing the weight reduces it.

- Specify multiple keywords for one group

Making a group by using single keyword may bring the group with various contents. Such a group can be divided into several appropriate groups by using multiple keywords simultaneously. We provide a manual operation to specify multiple keywords for a group with unique content.

4. Real-time description-answer short test system

We implemented the real-time description-answer short test system on Web, and used it in the lecture, "How to use the university library" which has 90 students.

The teacher asked, "How do you find Japanese books written about computer literacy in the Mie university library?" The purpose of the question was to make sure whether students know the following two issues or not. First, using the search-engine OPAC (On-line Public Access Catalog) is necessary to find required books in the Mie university library. Second, to find Japanese books, keywords for the OPAC must be written in Japanese.

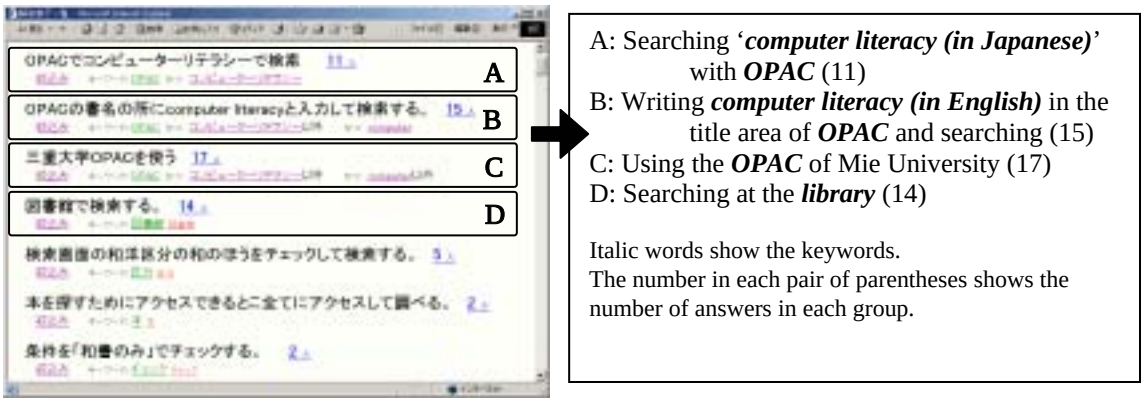

Figure 1: Result of classification

The result shown in the figure1, the teacher adjusting the weight three times and specifies multiple keywords two times. These operation was not a burden on the teacher.
The answers in the group A correspond to the answer that the teacher expected, because they include the both important keywords "OPAC" and "computer literacy (in Japanese)." The answers in the group B included the expected keyword "OPAC" and the unexpected keyword "computer literacy (in English)." The teacher advised to use the word "computer literacy (in Japanese)" to find Japanese books. The teacher gave the appropriate comments on the answers in the other groups, similarly.

5. Conclusion

We proposed a real-time description-answer short test system for teachers to be able to grasp students' comprehension in lectures. The system immediately classifies students' description-answers according to keywords extracted from them. The classified answers help teachers to grasp their comprehension. We applied this system to some large classes. We found this system was effective for grasping the comprehension.

Author's publications

[1] MORITA Naoki, KITA Hidehiko, TAKASE Haruhiko, HAYASHI Terumine, "多人数講義における記述式解答の内容を即時に把握するためのシステム", CIEC 会誌 コンピュータ&エデュケーション Vol.13, pp.103-109, 2002
[2] MORITA Naoki, KITA Hidehiko, TAKASE Haruhiko, HAYASHI Terumine, "記述式の解答を即時に講師が把握するためのシステム", FIT2002 情報科学技術フォーラム 情報技術レターズ vol.1, pp.233-234, 2002【FIT2002 論文賞受賞】
[3] MORITA Naoki, KITA Hidehiko, TAKASE Haruhiko, HAYASHI Terumine, "A Method of Immediately Classifying Description-Answers in a Large Class", International Conference on Computers in Education 2003, Proceedings CD-ROM 130-132, 2003

Studies on Pulverization of Fine Solid Particles by Super Sonic Jet Flow and Pneumatic Classification of Ultra Fine Solid Particles

Hiroshi Morimoto †
(Fluid and Thermo Engineering, Division of Systems Engineering)

Keywords : Fine and ultra fine solid particles, Gas-solid flow, Particle laden super sonic jet flow, Pulverization, Jet mill, Classification, Size distribution

1. Introduction

Recently, there are great requirements for ultra fine solid particles powder, in the fields of advanced materials, for example, electric parts in IT industry. Especially, the diameter control of fine powder is required. A super sonic jet mill or pneumatic type ultra fine powder classifier is used widely for the pulverization and classification of various kinds of fine particles in many powder manufacturing processes.

In pulverization by a jet mill, the improvement of pulverization efficiency is very important, because the jet mill consumes a large operating power. In classification by a pneumatic type powder classifier, there is no study on the flow characteristics which realizes a high performance for classification of ultra fine powder.

In this study, a new super sonic jet nozzle with a rectangular cross section is proposed and the flow and particle acceleration characteristics are investigated experimentally by velocity measurement and flow visualization. Numerical analysis is also carried out for reference. It was known that the new super sonic jet nozzle has a high performance for particle acceleration, namely for improvement of pulverization efficiency.

A new pneumatic type ultra fine powder classifier is also proposed and the relation between the performance and the flow characteristics is investigated by velocity measurements and flow visualization. The new classifier has a large swirling flow velocity, and then can classify ultra fine particles with sub-μm accuracy.

2. Results and Discussions

2.1 New super sonic jet nozzle with a rectangular cross section

Figure 1 shows a new supersonic jet nozzle with a rectangular cross section. In general, conventional supersonic nozzle has a round cross section then the flow spread three-dimensionally. But, new one has a rectangular cross section and then the flow spread two-dimensionally and the decay of the flow velocity will be suppressed. The particle acceleration performance and flow characteristics are examined experimentally by high-speed camera and Schlieren method, and the pulverization efficiency of fine particle is also tested for a few materials. The expansion angle and supplying air pressure are varied θ_i = 6 ° to 20 ° and P_0 = 0.2 to 0.6, respectively. It was known that the new supersonic nozzle has a high particle acceleration performance than the conventional one.

Figure 2 shows one example of the pulverization efficiency η of iron powder of mean diameter D_{50} = 62.4μm and density ρ = 7.85g/cm^3 which is obtained by a closed-circuit pulverization system. The new supersonic jet nozzle has 1.53 times processing rate of the conventional nozzle for the same products of D_{50} = 30μm. It has a high pulverization performance, especially for a large density materials, copper, iron and ruthenium.

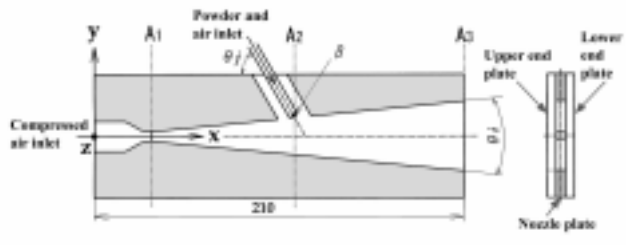

Fig.1 New super sonic jet nozzle

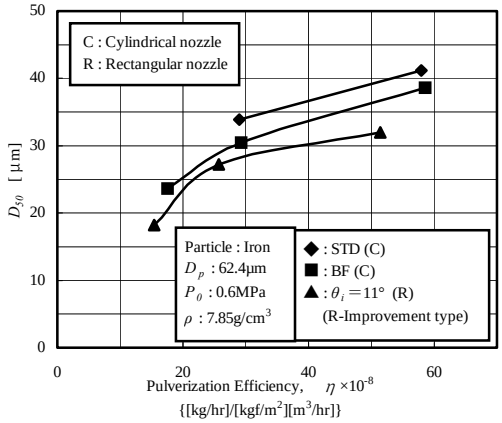

Fig.2 Pulverization efficiency

† Nippon Pneumatic MFG. CO., LTD

2.2 New pneumatic type ultra fine powder classifier

Figure 3 shows a new pneumatic type ultra fine powder classifier. It has conic shaped classification zone in order to generate a strong rotational flow. It was intended to realize an ideal flow field to give a large centrifugal force for all supplied fine particles in order to classify accurately in ultra fine powder. The flow condition was confirmed by flow visualization and observation by the tuft grid and oil dot methods and the measurement of air velocity distribution by a yawmeter with single hole. The classification performance was examined for some kinds of fine particles.

Figure 4 shows one example of the classification, partial separation efficiency, of calcium carbonate. The cutting size is D_{pc} = 0.95μm and sharpness index is SI = 1.98 when loading ratio is LR = 0.042, and then it can be said the classification performance is very fine. For some other materials, the good classification performance can be also obtained as follows. For tungsten dioxide, toner and barium titanate, D_{pc} = 1.23, 2.80, 2.45μm and SI = 1.22, 1.33, 1.16, respectively.

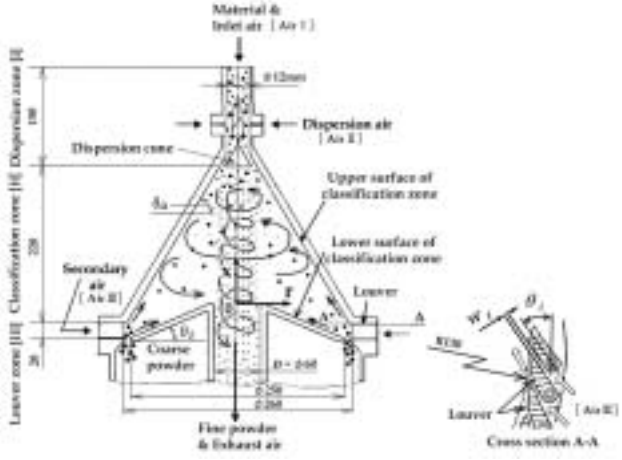

Fig.3 New ultra fine powder classifier

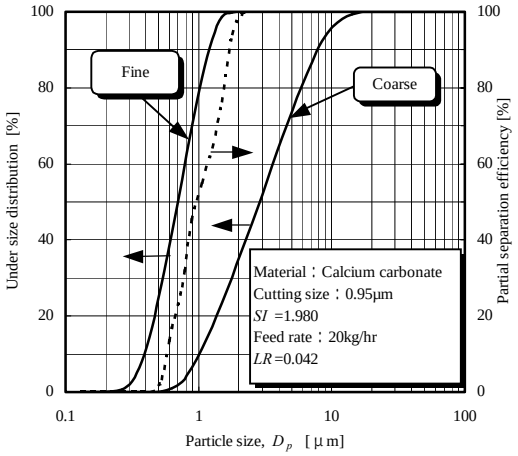

Fig.4 Classification of calcium carbonate

3. Concluding remarks

3.1 New super sonic jet nozzle with a rectangular cross section

i) The new super sonic jet nozzle has about 1.7 times a high performance for particle acceleration than that of the cylindrical nozzle.
ii) The numerical analysis agrees well with the flow visualization by Schlieren method.
iii) The new super sonic jet nozzle has a high pulverization performance for a large density material, copper, iron and ruthenium.

3.2 New pneumatic type ultra fine powder classifier

i) The flow introduced into the classification zone passing through the louvers, which were set evenly on the circumference at the bottom of the conic, is divided into two flows which flow on the upper and lower surfaces. The upper flow is swirling up along the upper surface and after turning at the top of the conic it is exhausted from the exit.
ii) The descending flow area near the center forms the maximum swirling velocity (the fastest tangential velocity) region in the classification zone.
iii) The new pneumatic type ultra fine powder classifier can classify the ultra fine powder very accurately.
iv) The approximate theory for the cutting size can express the experimental one well.

Author's publications

[1] H. Morimoto, N. Oda, H. Terada, and T. Shakouchi, *Inner Flow of Pneumatic Powder Separator and Separation Efficiency*, Trans of JSME, No.973-1, pp.249-250, Mar., 1997
[2] H. Morimoto, *Air Pulverizing, Classification and Dispersion*, Seminar's Materials of Tokai Branch of The Heat Transfer Society of Japan, pp.39-54, Oct., 2000
[3] H. Morimoto, T. Shakouchi, *Study on Flow Characteristics in and Classification Efficiency of Pneumatic Type Ultra Fine Powder Classifier*, Trans. of JSME, 68-668 B, pp140-146, Apr., 2002
[4] H. Morimoto, T. Shakouchi, *Classification of Ultra Fine Powder by a New Pneumatic Type Classifier*, Powder Technology, Vol.131/1, pp71-79, Nov., 2002
[5] H. Morimoto, T. Shakouchi, *Flow Characteristics and Classification Efficiency of New Pneumatic Type Ultra Fine Powder Classifier*, 4th World Congress on Particle Technology, CD-ROM, Jul., 2002

Automatic text classification of English newswire articles based on statistical classification techniques

Zu Guowei†

Keywords：automatic text classification, principal component analysis, projection distance, variable transformation

1. INTRODUCTION

The basic process of automatic text classification is learning a classification scheme from training examples then using it to classify unseen textual documents. In this paper, we focus on techniques of feature transformation such as the normalization to the relative word frequency, the principal component analysis (PCA) and the power transformation to improve the accuracy and the speed of automatic text classification.

In order to evaluate the effectiveness of the variable transformation and the principal component analysis, Several classification techniques based on the Euclidean distance, Fisher's linear discriminant function, projection distance, modified projection distance and the support vector machine (SVM) are employed in the classification test for the English text collection (the reuters-21578).

Furthermore, we perform automatic text classification experiments for English newswire articles to study on the relationships between the accuracies of OCR and the text classification employing the statistical classification techniques.

2. THE BASIC TECHNOLOGY

In this research we employed the statistical classification technique for classifying a feature vector composed of frequencies of lexicon words that appear in a text. The approach is learning a classification scheme from labeled training examples then using it to classify unseen textual documents. Several classification techniques based on the Euclidean distance, Fisher's linear discrimination function, projection distances, and the support vector machine (SVM) are employed in the classification test for the English text collection (the reuters-21578).

A drawback of the statistical classification technique is that the dimensionality of the feature vector can increase together with the lexicon size. For example, the lexicon size and the feature dimensionality grow to 34,868 for Reuters-21578 articles, which requires enormous computational time and storage for the text classification. To solve this problem we need to employ a statistical feature extraction technique which extracts small number of features with high separability to reduce the feature dimensionality without sacrificing the classification accuracy. In this research the dimension reduction based on the principal component analysis (PCA) was employed.

The word frequency is widely used as the basic feature in the statistical text classification approach. Since the absolute frequency depends on the length of the text, the relative frequency which does not depend on the length is also employed. Because the relative frequency does not depend on the text length, the within-class variance of the relative frequency is smaller than the absolute frequency. Therefore we can expect that separability in the feature space and the classification rate is improved when the relative frequency is employed

Another variable transformation, the power transformation is employed to improve the classification accuracy. This transformation improves the symmetry of the distribution of the frequency which is noticeably asymmetric near the origin.

3. THE CLASSIFICATION EXPERIMENT

Classification experiments were performed to comparatively evaluate the feature extraction and classification techniques using the data collection Reuters-21578, which is composed of 21578 articles manually classified to 135 categories. In the experiments total of 750 articles, 150 articles/category randomly selected from five categories (acq, crude, earn, grain, trade), were used.

Fig.1 shows the relationship between the average classification rate and the dimensionality of the feature vector composed of the absolute word frequencies. Fig.2 shows the classification rate at the optimal feature dimensionality. And Fig.3 shows the relationship between the text classification rate and the word recognition rate.

† Division of Systems Engineering, Mie University

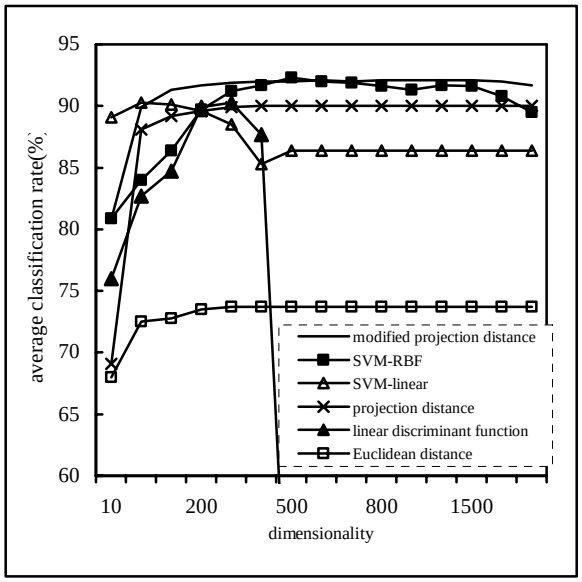

Fig. 1. Classification rate vs. dimensionality (absolute frequency)

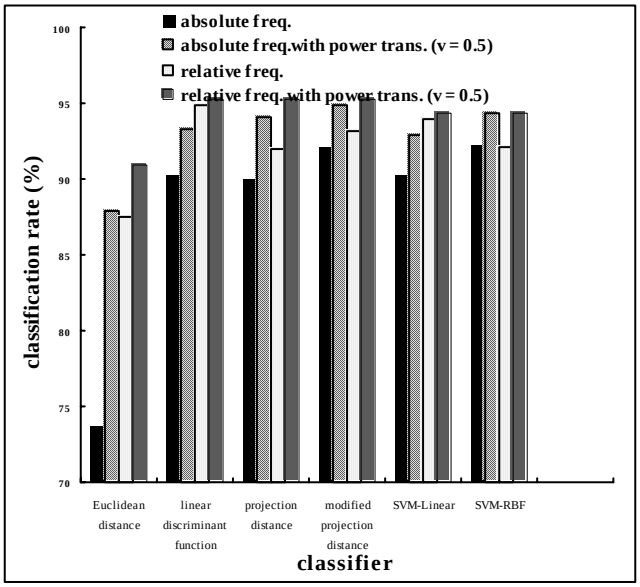

Fig. 2. Classification rate at the optimal feature dimension

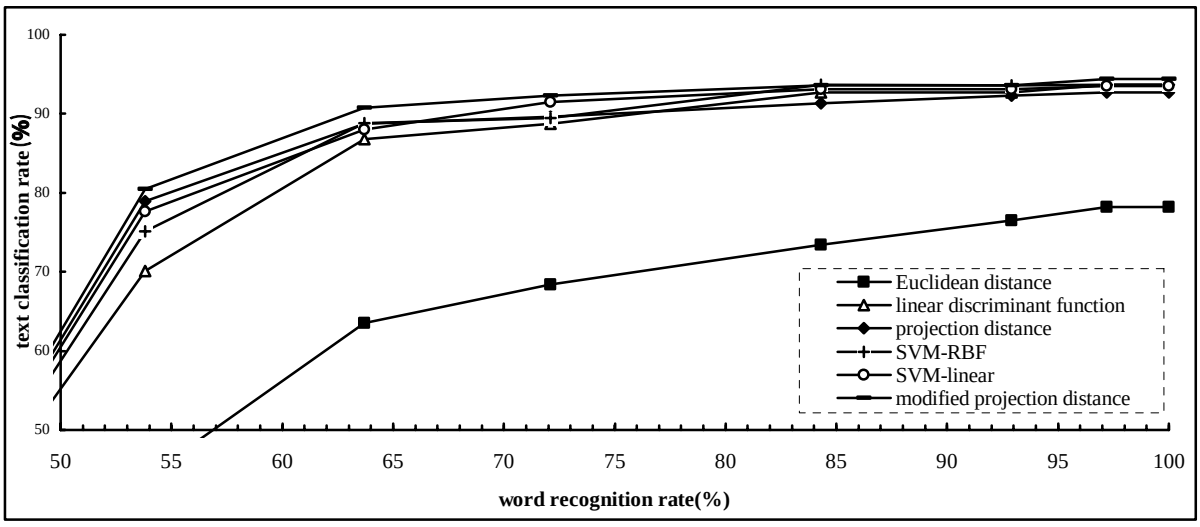

Fig.3 The relationship between the text classification rate and the word recognition rate

4. THE RESULTS OF EXPERIMEN

The results of experiment are summarized as follows:

(1) the principal component analysis drastically reduced the feature dimensionality without sacrificing the classification performance,

(2) the normalization to the relative frequency followed by the power transformation improved the classifier performance significantly,

(3) considerably high classification rate for the transformed features was achieved by the modified projection distance, and

(4) the text classification rates of all classification techniques were not deteriorated significantly until the word recognition rate was deteriorated to 95% or 80%, respectively. And the modified projection distance outperformed the others in the accuracy and the robustness of the text classification in this experiment.

AUTHOR'S PUBLICATION

1. Guowei Zu, Wataru Ohyama, Tetsushi Wakabayashi, Fumitaka Kimura, "Automatic text classification of English newswire articles based on statistical classification techniques" *IEEJ Trans. EIS*, Vol.124, No3, pp.852-860, 2003

2. Guowei Zu, Wataru Ohyama, Tetsushi Wakabayashi, Fumitaka Kimura, "Accuracy improvement of automatic text classification based on feature transformation" *DocEng'03* (ACM Symposium on Document Engineering 2003), pp.118-120,November 20–22, 2003, Grenoble, France

LCA Consolidated Evaluation of Indonesian Electricity Generation Systems

Anugerah Widiyanto
(Energy Systems Design, Division of Systems Engineering)

Keywords: Power plants, Energy conversion, Environmental impacts, Life cycle assessment, Life cycle inventory, Indonesia, Electric generation systems, LCA-NETS method

1. Introduction

The life cycle inventory (LCI) data of the electric power generation plays a vital role on LCIs of the industrial products. However there are no formal life cycle assessment (LCA) studies in Indonesia so far due to limited number of LCA expertise and lack of sufficient databases relevant to domestic conditions. Therefore, the aim of this study is, firstly to introduce life cycle assessment methodology for Indonesian electric power generation systems, secondly to establish LCI data for electricity grid mix of Indonesia, and finally, to evaluate the environmental from a life cycle impact assessment (LCIA) point of view.

A model was developed for the analysis, which had advantages of being based on new reliable data reflecting the current status in Indonesia with a combined method of process analysis and input-output analysis. Using the developed model, the life cycle emissions per kWh of electricity of CO_2, SO_2, NOx, CO, CH_4, NMHC, N_2O, Dust (SPM), Ni, As, Cd, Cr, Hg, Pb, and Zn were studied in a cradle-to-grave manner. The proposed LCA-*NETS* (Numerical Eco-load Total Standard) method is used as life cycle impact assessment method. As the results the LCA evaluations are discussed for further ecological improvement.

2. Methodology

2.1. Life cycle inventory data

In this LCA, the life cycle emission factor LCE_i was used as an index to evaluate the selected emission characteristics of the power generation technologies from the lifecycle viewpoint. The amount of emissions released across the entire life cycle to generate net 1 kWh of electricity is defined as follows:

$$LCE_i = \frac{\sum_i Df_i + Dc_i + Do_i + Dd_i}{Eg} \quad (1)$$

Where: *Df* is direct discharged emission caused by the combustion of fossil fuels in power plants. *Dc* is discharged emission associated with the construction of plants required in the system studied. *Do* is discharged emission for operation and maintenance for the plants. *Dd* is discharged emission by decommissioning the plants. *Dc*, *Do* and *Dd* are here referred to as indirect discharged emissions. Subscript *i* indicates the type of emission (CO_2, SO_2, NOx, CO, CH_4, NMHC, N_2O, Dust, Ni, As, Cd, Cr, Hg, Pb, Zn). *Eg* is net output of electricity during a lifetime of a power plant. Net output is the amount of electricity supplied to the grid excluding the energy consumption for the operation of the plants.

2.2. Life cycle impact assessment method

In the LCA-*NETS* method, the analyzation of an environmental load is expressed by standardizing on the basis of the L-R Tolerance Balance Theory, which balances the maximum tolerable value that the Loader can emit or consume, and the maximum value that the Receiver affected by the load can tolerate. This approach has the additional feature of allowing a complete quantitative evaluation of the various environmental loads in the new units [NETS]. The L-R Balance Theory defines, first of all, the Maximum Permissible Eco-load Value (MEV_j) [NETS] for given environmental load (*j*) tolerated by the ecosystem on the Receiver side. In this scheme, the tolerable value for a person is determined as 100 [NETS], because the tolerance level has reached 100%, and unless some measure is taken, the standard of living we have enjoyed so far cannot be maintained. When the maximum tolerance value is P_j (kg, kWh, m^3, etc.), according to the L-R Tolerance Balance Theory,

$$P_j \cdot ELM_j = MEV_j \quad (2)$$

here, ELM_j [NETS/kg, kWh, m^3, etc.] (Environmental Load Module) is the conversion coefficient connecting P_j [kg, kWh, m^3, etc.] and MEV_j [NETS], and also refers to the environmental load consolidated basic value for unit emission or consumption.

3. Results and Discussion

In this study, the life cycle inventory (LCI) for electricity grid system in Indonesia was developed and evaluated based on PLN data of fiscal year 2001. Figure 1 shows the composition of electricity generation in Indonesia classified by power plant type. Figure 2 presents a comparison of the life cycle GHG emissions and its composition per region. As the LCI result, the average amount of emission intensities [kg/kWh] for main emissions of CO_2, SO_2, NOx, CO, CH_4, NMHC, N_2O, Dust (SPM), Ni, V, As, Cd, Cr, Hg, Pb, Zn were 7.2×10^{-1}, 2.4×10^{-3}, 3.0×10^{-3}, 1.2×10^{-4}, 4.5×10^{-3}, 7.2×10^{-4}, 2.3×10^{-5}, 2.7×10^{-4}, 7×10^{-7}, 1×10^{-6}, 2×10^{-8}, 2×10^{-9}, 2×10^{-8}, 1×10^{-8}, 4×10^{-8}, and 1×10^{-7}, respectively. Compared to Japan, these values of CO_2, SO_2, NOx, CO, CH_4, NMHC, N_2O, Dust (SPM) are 167%, 615%, 714%, 92%, 321%, 218%, 209%, 1000%, respectively those of Japan. As for heavy metals emissions, compared with Japan, these values are about 489% to 3258%. And the average environmental load consolidated value that has been calculated using LCA-NETS method for Indonesian grid electricity system is found of 2.7×10^{-3} [NETS/kWh].

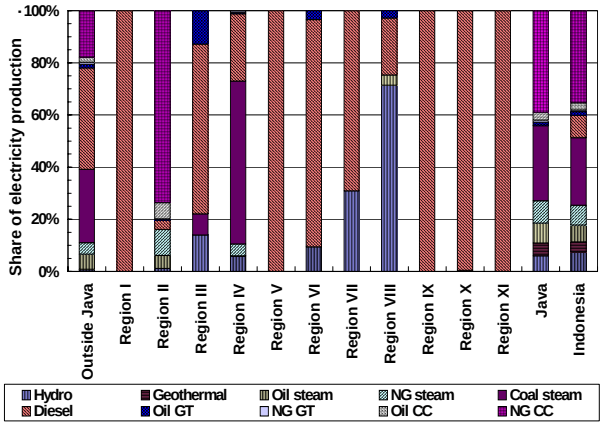

Fig. 1: Share of electricity production per region

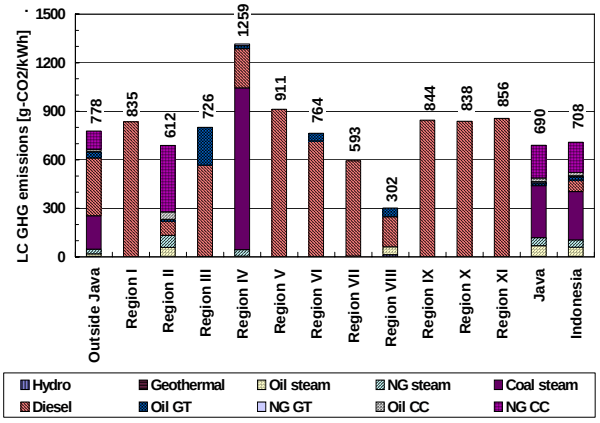

Fig. 2: Life cycle GHG emissions per region

4. Concluding Remarks

We have conducted a quantitative analysis of the environmental load produced by energy systems such as various kind of power plants and co-generation systems using the LCA-*NETS* approach developed by the authors' laboratory. We also have evaluated the environmental load produced by various types of energy system in terms of environmental load consolidated values that cover the entire LC phases. This result could be useful for further LCA research.

Author's main publications

[1] A. Widiyanto, S. Kato, N. Maruyama, *Environmental Impact Analysis of Indonesian Electric Generation Systems*, JSME International Journal, Series B, Vol. 46, No. 4 (November 2003), pp. 650-659.

[2] A. Widiyanto, S. Kato, N. Maruyama, Y. Kojima, *Environmental Impacts of Fossil Fuel Fired Co-Generation Plants Using A Numerically Standardized LCA Scheme*, ASME Transactions, Journal of Energy Resources and Technology, Vol. 125, No. 1 (March 2003), pp. 9-16.

[3] A. Widiyanto, S. Kato, N. Maruyama, *A LCA/LCC Optimized Selection of Power Plant System with Additional Facilities Options*, ASME Transactions, Journal of Energy Resources and Technology, Vol. 124, No. 4 (December 2002), pp. 290-299.

[4] S. Kato, N. Maruyama, Y. Nikai, H. Takai, A. Widiyanto, *Life Cycle Assessment Estimation for Eco-Management of Co-Generation Systems*, ASME Transactions, Journal of Energy Resources and Technology, Vol. 123, No. 1 (March 2001), pp. 15-20.

[5] A. Widiyanto, S. Kato, *Life Cycle Assessment of Power Generation Systems*, Journal of Fusii, Special Edition, No. 6 (March 2000), pp. 72-76.

[6] S. Kato, N. Maruyama, Y. Nikai, H. Takai, Y. Kojima, A. Widiyanto, *Quantitave Standardization of Various Global Environmental Loads and Its Applications to Eco-load Operation Scheme of Co-generation Systems* (in Japanese), Journal of Fluid and Heat Eng. Research, Vol. 34, No. 2 (December 1999), pp. 37-44.

[7] A. Widiyanto, S. Kato, N. Maruyama, *Optimizing Selection of Appropriate Power Generation Systems in Indonesia By Using Distance Based Approach Method*, ASME Transactions, Journal of Energy Resources and Technology, Vol. 126, No.1, (in press).

[8] A. Widiyanto, S. Kato, N. Maruyama, *Development of Decision Model for Selection of Appropriate Power Generation System Using Distance Based Approach Method*, JSME International Journal, Series B, Vol. 47, (in press).

[9] S. Kato, A. Widiyanto, *Environmental Impact Consolidated Evaluation of Energy Systems by a LCA-NETS Scheme*, Elsevier, Energy, The International Journal, Vol. 29, (in press).

[10] A. Widiyanto, S. Kato, N. Maruyama, *LCA Consolidated Evaluation of Indonesian Electricity Grid System (Part 1: Evaluation of Green House Gas Emissions from Power Generation Systems)*, The International Journal of Life Cycle Assessment, (accepted).

[11] A. Widiyanto, S. Kato, N. Maruyama, *LCA Consolidated Evaluation of Indonesian Electricity Grid System (Part 2: Development of Life Cycle Inventory)*, The International Journal of Life Cycle Assessment, (accepted).

A Study on Harmonics Suppression of PMSM Using Repetitive Control and Application to Improvement of Sensorless Control Performance

Jeong-Seong Kim †

Key Word : Permanent magnet synchronous motors, Harmonic currents, Repetitive control, Sensorless Control

Ⅰ. INTRODUCTION

In recent years, PMSMs (Permanent Magnet Synchronous Motor) have been widely used for industry applications and home electric appliances. PMSMs are generally driven by the vector control system based on the current control. However, there are some harmonic components in the current control loop of vector control system. These harmonic currents bring about problems such as decrease of control performance and vibration of the motor, and they have bad influence on sensorless control.

In this paper, we propose a control method suppressing all harmonic current components using the repetitive control. Furthermore, in this paper, we show that the proposed control system can be used for improvement of position/velocity sensorless control performance. The one of important features of the harmonics suppression control system is that harmonic components of not only currents but also voltage commands can be suppressed. So, it can be expected that estimation ability of the sensorless control system would be improved.

Ⅱ. CONFIGURATION OF THE CONTROL SYSTEM

Fig.1 shows the configuration of the proposed harmonics suppression control system. The compensation signal learning process to suppress harmonics in the current control loop is as follow. First, harmonic component $v^*_{dq(h)}$ extracted from *d-q* coordinate voltage command v^*_{dq} is put into the repetitive compensator (*N* memories) as a source of compensation signal. In the repetitive compensator, the input signal is added to the output one delayed by one cycle. k_1 is set as 0, that is, the proposed control system doesn't need to adjust the phase of compensation signal for the stabilization of the repetitive control. The compensation signal v_{dq_c} made through above process is added to original voltage command v^*_{dq}. The learning process for compensation signal is repeated until harmonics are suppressed fully, suppressing harmonics in the current control loop and building up the compensation signal. Removal of DC component is carried out by HPF [$HPF(s) = \tau s/(\tau s+1),\ (1/\tau = \omega_{re})$].

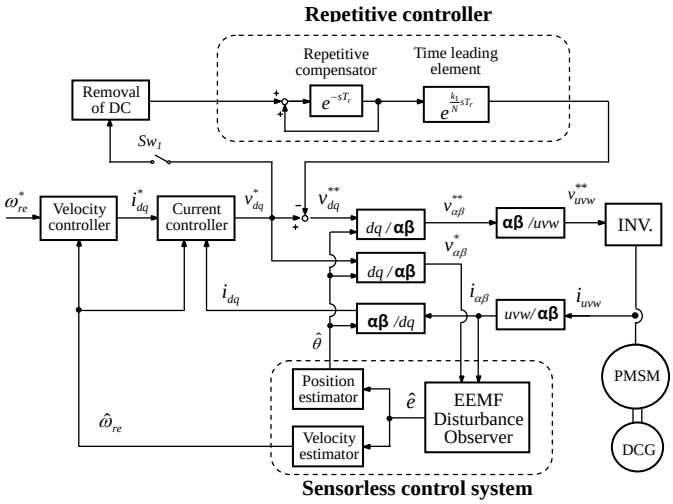

Fig.1 Configuration of the proposed control system

According as harmonic components in v^*_{dq} are reduced, $i_{\alpha\beta}$ and $v^*_{\alpha\beta}$ nearly approach to the sine wave as shown in Fig.2. With these $i_{\alpha\beta}$ and $v^*_{\alpha\beta}$, we construct sensorless control system which is based on the extended EMF disturbance observer as an example. As a result of suppression harmonics, we can have margin in the pole assignment of observer so that the performance of sensorless control can be improved.

† Dept. of Electrical and Electronic Eng., Mie University

Ⅲ. EXPERIMENTAL RESULTS

Fig.2 shows experimental results when electrical rotation velocity is 100[rad/s] and the cut-off frequency of current control system is 1500[rad/s]. From Fig.2, we can confirm that the proposed control system excellently suppresses harmonic currents, so currents of the α β axis become almost sine waves. Fig.3 shows the experimental results of senseless control drive. Fig.3(a) and (b) is the case without repetitive control, when observer pole is placed at $0.25\,|\hat{\omega}_{re}|$ and $2.0\,|\hat{\omega}_{re}|$ respectively. Fig.3(c) is with repetitive control, when observer pole is $2.0\,|\hat{\omega}_{re}|$. Left side of the figure is result of steady state drive, when velocity is of 50rad/s. Right side of the figure is acceleration and deceleration drive, that is step changes between 50rad/s and 200rad/s. From Fig.3(a) and (b), we can confirm performance trade-off caused by the pole assignment. However, in case that observer pole is assigned largely ($2.0\,|\hat{\omega}_{re}|$) after harmonic suppression with repetitive control, it is possible to enhance the estimation ability as good as Fig.3(a) on the steady state, keeping estimation ability on the transient state as shown in Fig.3(c).

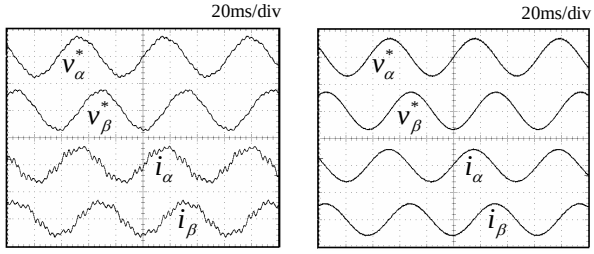

(a) without repetitive control (b) with repetitive control

Fig.2 Waveforms when with and without repetitive control (100rad/s, Ch1,2:100V/div Ch3,4:2.5A/div)

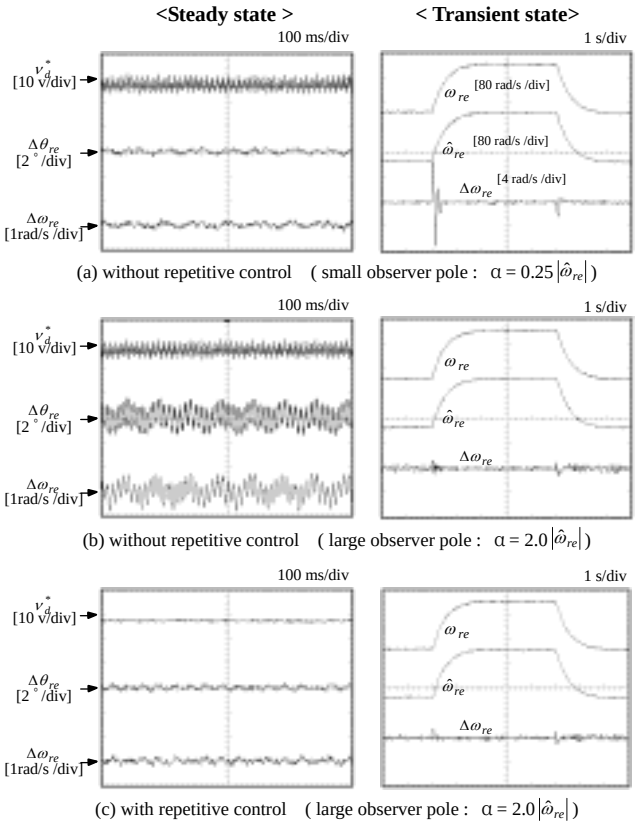

(a) without repetitive control (small observer pole : $\alpha = 0.25\,|\hat{\omega}_{re}|$)

(b) without repetitive control (large observer pole : $\alpha = 2.0\,|\hat{\omega}_{re}|$)

(c) with repetitive control (large observer pole : $\alpha = 2.0\,|\hat{\omega}_{re}|$)

Fig.3 Improvement of position and velocity estimation ability by suppression of harmonic components

Ⅳ. CONCLUSIONS

We proposed an improving method of sensorless control performance for the PMSM by suppression of harmonic components of the vector control using the repetitive control. The sensorless control system for the PMSM was constructed based on the observer with the current and voltage command whose harmonic components were suppressed by the repetitive control. As a result, we could have a margin in pole assignment of the observer so that the performance of sensorless control could be improved. The experiments showed that the proposed method is effective.

Author's main publications

[1] Jeaong-seong Kim, Shinji Doki, Muneaki Ishida : "Improvement of IPMSM Sensorless Control Performance by Suppression of Harmonics on the Vector Control Using Fourier Transform and Repetitive Control", CD-ROM of the 28th International Conference on Industrial Electronics, Control and Instrumentation, (IECON'02, Sevilla, Spain), (2002/11)

[2] Jeaong-seong Kim, Shinji Doki, Muneaki Ishida : "Suppression of Harmonic Current in Vector Control for IPMSM by Utilizing Repetitive Control", Proceedings of the 2002 IEEE International Conference on Industrial Technology, (ICIT'02, bangkok, Thailand), Vol.1, pp.264/267, (2002/12)

[3] Jeaong-seong Kim, Shinji Doki, Muneaki Ishida : "Harmonics Suppression of PMSM Using Repetitive control and Application to Improvement of Sensorless Control Performance", CD-ROM of the 29th International Conference on Industrial Electronics, Control and Instrumentation, (IECON'03, Roanoke, USA), (2003/11)

[4] Jeaong-seong Kim, Shinji Doki, Muneaki Ishida : "Improvement SensorlessControl Performance for IPMSM by Suppression of Harmonic Current with Fourier Transform and Repetitive Control", Trans. IEE of Japan, Vol.123-D, No.10, pp.1176/1184 (2003/10)

Study of Trenchless Buried Objects Survey and Non-Destructive Testing Method for Underground Tele-Communication's Equipment

Yoshikazu Sudo †

Keyword: Underground Radar, GPR, Non-Destructive Testing, Frequency analysis, Pattern recognition

1. INTRODUCTION

Ground penetrating radar offers an effective means for conducting underground surveys at relatively shallow depths. The problem, however, is that skill is required to interpret the resulting imagery. This makes it difficult to process large volumes of data quickly, which has impeded expansion of the range of use of ground penetrating radar.

The authors have investigated methods to isolate only the specific signals of buried objects by using the previously identified frequency domain characteristics of ground penetrating radar wave reflections in order to simplify image interpretation and to enable speedy processing of large volumes of data [1]-[3]. The authors had recognized that the reflected waves from buried pipes and from underground cavities are distributed to specific areas in the frequency domain, and pointed out the possibility of isolating the signals from buried pipes and cavities. They had further pointed out that buried objects and cavities differ from each other in the frequency feature distributions with respect to the hyperbolic curves of signals , that is, their distributions with respect to the directional angle of received waves.

This paper describes aerial experimental results of radar surveys of steel pipe and steel plate conducted in order to study their characteristics as part of a wide range of basic study to determine the reasons for the difference in frequency domain characteristics between buried pipe and underground cavities.

2. EXPERIMENTAL APPARATUS and CONDITIONS

Figure 1 shows the experimental conditions. A semicircle as shown in Figure 1 was drawn on the ground surface and the ground penetrating radar antenna was placed at its center. Two measuring lines—line A, on the semicircle, and line B, a tangent line parallel to the antenna—were drawn. The directional angle θ was set as shown in Figure 2, and objects were placed at the points where a line in the radial direction intersects with lines A and B. Two objects were used, a 100-mm diameter steel pipe and a 500 X 1000-mm steel plate. The steel plate was fixed so that its flat surface was oriented vertically and its long side was parallel to line B.

The waves from the ground penetrating radar reflected from the steel pipe and steel plate, respectively, were observed under these conditions. The system involves a function to isolate only the signals of the observed waves reflected from the objects, from which the corresponding frequency spectra were calculated, and their central frequencies and half-widths were derived.

3.RESULTS and DISCUSSION

Figure 2 shows the observed central frequency and half-width on line A. In the case of the steel pipe, the central frequency showed little change until the directional angle reached the vicinity of 30°. The half-width tended to increase as the directional angle increased from 0°. When the directional angle exceeded 40°, each feature value showed a rapid drop. It is considered that this drop has been resulted from the rapid decrease in energy owing to the directivity of the transmitted electromagnetic pulse, and it is unlikely to be a distinctive characteristic of the steel pipe. In the case of the steel plate, on the other hand, both feature values seemed not to depend on the directional angle. Figure 3 shows the observed central frequency and half-width on line B. Where both the central frequency and half-width tended to increase with the directional

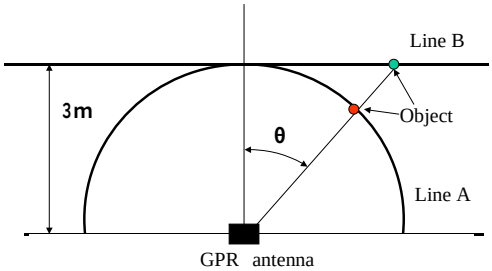

Object : Steel pipe φ100

Steel plate 500×1000, t=3.0 (mm)

Fig.1 Experimental Condition

† AIREC Engineering Co.

angle up to about 30° in the case of the steel pipe, they showed the opposite tendency to decrease in the case of the steel plate.

In Figures 2 and 3, the central frequency and half-width in the vicinity of a 0° directional angle both show larger values in the case of the steel plate. This is thought to be because, whereas the transmitter antenna is markedly larger than the steel pipe, it is about the same size as the steel plate, and also because the steel plate is directly opposed to the antenna, so that there was less disorder in the reflected wave.

Tests previously conducted by the authors showed both the central frequency and the half-width reaching higher levels with a plate-shaped cavity than with a buried pipe. Those findings closely match the present results. In the case of an actually buried pipe, the signals from showed a tendency for both the central frequency and half-width to decrease as the antenna approached a point directly above the buried pipe, while that in the case of a cavity showed the reverse increasing tendency. The present results match closely with these observations.

The difference observed in the present experiment is thought to originate from the shape difference between the steel pipe and steel plate, since both are made of the same material. This suggests that it is possible to recognize shapes of objects using the present results. Clarification of this possibility, however, will require more detailed study that varies the shapes, sizes, and materials of the objects.

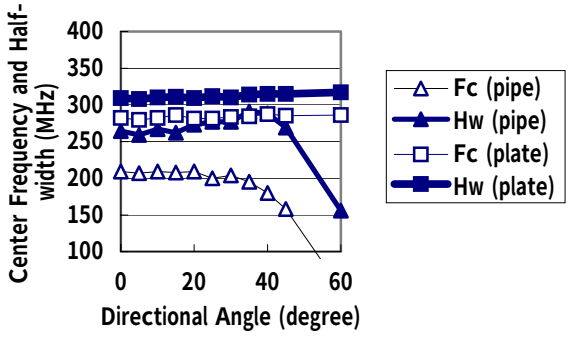

Fig2. Relationship of Fc and Hw to Directional Angle, line A

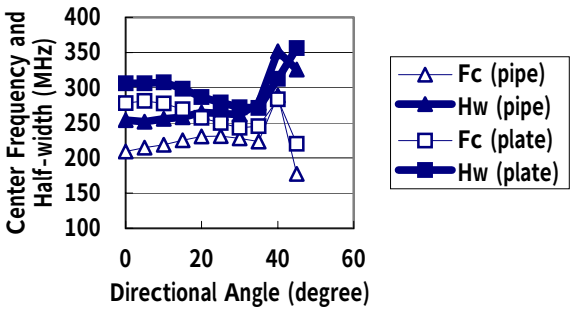

Fig.3 Relationship of Fc and Hw to Directional Angle, line B

4. CONCLUSION

Experimental investigation of the relationship between the central frequency and half-width of a reflected wave and its directional angle when using ground penetrating radar aerially yielded the following observations:

(1) The central frequencies and half-widths of waves reflected from pipe and steel plate tend to differ. This tendency coincides with the results from actual buried objects such as steel pipe and steel plate.

(2) The reason for this tendency to differ is thought to be the different shapes of the objects.

(3) The current results confirmed the possibility that shapes of objects buried in the ground could be recognized, but this will require further, more detailed study involving varying shapes, sizes, and materials.

Authors Publications

[1] H. Akutsu, Y. Nagashima, J. Masuda, S. Kohno and Y. Sudo; " Development an Underground Radar System," No-Dig Oosaka, 1990, L4.1-L4.8.

[2] Y. Sudo, Y. Nomura and Y. Nagashima, "A Cavity Signal Recognition Method using Spectrum Pattern Analysis in GPR Received Wave," Mechanical Engineering Congress, 2002 Japan, Vol.Ⅶ, pp239-240.

[3] Y. Sudo, Y. Nomura and Y. Nagashima, "Extraction of Cavity Signals from Underground Radar Images Using Frequency Analysis," The 6th International Conference on Mechatronics Technology, ICMT2002, 2002, pp.129-134

Preparation and Interface Properties of Highly Purified Polyglycerol Fatty Acid Esters

Tomoharu Kato*

Key Words: CMC, detergency, foam, interface property, monolayer, polyglycerol ester, polyglycerol monolaurate, poluglycerol monostearate, surface activity, surface pressure-area isotherm, surfactant property.

Polyglycerol esters of fatty acids (PGE), nonionic surfactants, are widely used in foods, cosmetics, and other industrial products. The PGE consists of polymerized glycerol units and fatty acids. The commercial form of PGE is in general a mixture of many different components, which include different glycerol units from 1 to 10 with various degrees of esterification with fatty acids of different chain lengths. Efforts have been made to purify the PGE to characterize the surfactant properties of individual polyglycerol. The purification process of the mixture was not easy, and hence most studies restricted their discussion on the properties of the mixture itself. Surfactant properties of a surfactant in aqueous solution are important for characterization. It is therefore, necessary to know the surfactant properties of the purified glycerol units.

1. The purpose

In this study, several PGE were purified and then characterized their surfactant properties in aqueous solutions.

2. Synthesis of purified polyglycerol esters of fatty acids

Stearic and lauric acid were selected as the fatty acids of PGE. The polyglycerols were purified by silica gel column to yield the esters, which were composed with fatty acid derivatives. The esterified products were further purified once again with silica gel column. As a result, highly purified (>95%) di- and triglycerol monostearates (2GMS and 3GMS), and di- to pentaglycerol monolaurates (2GML, 3GML, 4GML and 5GML) were obtained. The purity of each polygycerol was checked by gas liquid chromatography. Chain lengths were confirmed by infrared spectrum, nuclear magnetic resonance spectrum, chemistry ionizing mass spectrum and atmospheric pressure chemistry ionizing mass spectrum.

3. Surface properties of mono-, di-, and triglycerol monostearate monolayers spread at the air/aqueous solution interface

The monolayer properties of three polyglycerol monostearates spread at the air-water interface were measured by surface pressure measurement and fluorescence microscopy observation as a function of glycerol units from 1 to 3. Polyglycerol monostearates formed stable monolayers at the air/aqueous solution interface and the shape of the surface pressure-area (π-A) isotherms of the monolayers showed a strong dependence on the glycerol units (**Fig.1**). Glycerol monostearate (1GMS) showed a typical liquid-condensed (LC) monolayer, 2GMS showed a monolayer with a phase transition from liquid-expanded (LE) to LC states, and 3GMS exhibited LE type monolayer. The collapse surface pressure decreases with an increase in the number of glycerol units. The fluorescence microscopic images of polyglycerol monostearate monolayers are also strongly depended on the number of glycerol units. When the monolayer of 2GMS

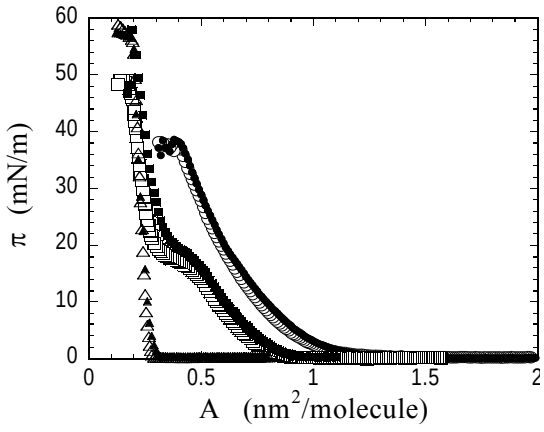

Fig.1 Surface pressure -area (π -A) isotherms of 1GMS (triangles), 2GMS (squares), and 3GMS (circles) monolayers in the abcence (open symbols) and presence (closed symbols) of NBD-PE at 25 ℃

* Taiyo Kaguku Co.,Ltd.

is compressed into the LE to LC phase transition, its domain structure changed from circular to radial cusp shape via horse-bean shape, whereas the domain structure of 1GMS turned from circular to coalesced circular shape with a decrease in the area.

4. Surfactant properties of purified polyglycerol monolaurates

Surfactant properties, such as surface activity, foaming property, interfacial tension, and detergency of the purified polyglycerol monolaurates (nGML) in aqueous solutions were systematically examined and were compared with the corresponding properties of n-dodecyl polyoxyethylene monoethers ($C_{12}EOn$). The values of critical micelle concentration (CMC) and the surface tension at CMC of nGML and $C_{12}EOn$ were increased linearly with an increase in the number of glycerol and oxyetylene units, respectively and the slope of the increase was greater for nGML than $C_{12}EOn$. The minimum surface area per molecule of nGML was smaller than that of $C_{12}EOn$ at the air/aqueous solution interface. The initial foam heights of the surfactants at the CMC were increased with the increase in the number of glycerol or oxyetylene units and the foam heights of nGML were always higher and stable than that of $C_{12}EOn$. Detergency depended on interfacial tension reduction, 3GML showed the lowest interfacial tension and the highest detergency among all the surfactants tested (**Fig.2**).

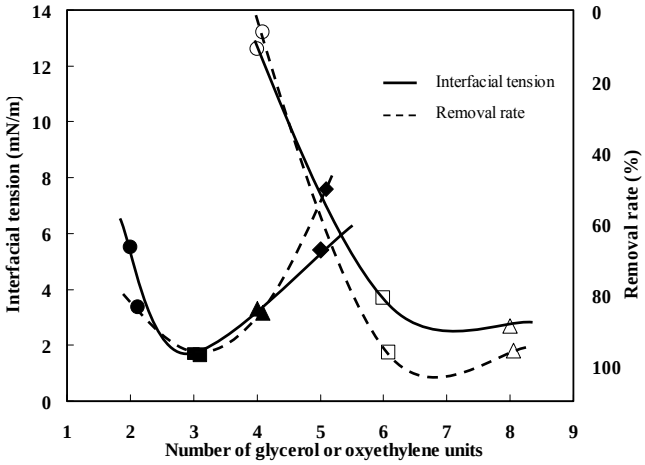

Fig.2 Plots of interfacial tension of corn oil/surfactant solutions and detergency as a function of the number of glycerol or oxyethylene unites for 2GML (●), 3GML (■), 4GML (▲), 5GML (◆), $C_{12}EO_4$ (○), $C_{12}EO_6$ (□) and $C_{12}EO_8$ (△) in aqueous solutions at 30ºC

Overall, the nGML showed better performance in all the surfactant properties than $C_{12}EOn$. It is noteworthy that the surfactant properties of nGML having few glycerol units (di- to tetraglycerol monolaurate) are on par with that of $C_{12}EOn$ having many oxyetylene units (hexa- and octaoxyethylene). These results suggest that nGML having a secondary hydroxyl group on every glycerol unit of the hydrophilic part could be more hydrophilic than $C_{12}EOn$. This characteristic feature guaranteed the superior surfactant properties of nGML. This study suggests that the purified nGML have excellent surfactant properties relative to their ethoxylated analogues. nGML are suitable for use as detergents in foods, cosmetics and in other industrial materials.

5. Conclusion

1) Highly purified 1GMS to 3GMS and 2GML to 5GML were characterized their interface properties.
2) Surface properties of 1GMS to 3GMS monolayers spread at the air/aqueous solution interface strongly depended on the number of glycerol units.
3) Surfactant properties, such as surface activity, foaming property, interfacial tension, and detergency of the purified nGML in aqueous solutions strongly depended on the number of glycerol units. Overall, the nGML showed better performance in all the surfactant properties than $C_{12}EOn$. These results suggest that nGML having a secondary hydroxyl group on every glycerol unit of the hydrophilic part could be more hydrophilic than $C_{12}EOn$.
4) PGE could be an abundant source of surfactants because they could be produced from plant sources. Therefore, nGML could form as the interesting surfactants for the future.

Author's publications

1. Masami Kawaguchi, Midori Yamamoto, Takeshi Nakamura, Masatsugu Yamashita, Tomoharu Kato, and Tadaya Kato, "Surface Properties of Mono-, Di-, and Triglycerol Monostearate Monolayers Spread at the Air-Water Interface", *Langmuir*, 17, 4677-4680 (2001).
2. Tomoharu Kato, Takeshi Nakamura, Masatsugu Yamashita, Masami Kawaguchi, Tadaya Kato, and Takahito Itoh, "Surfactant Properties of Purified Polyglycerol Monolaurates", *Journal of Surfactant and Detergency*, 6, 331-337 (2003).

Studies on the development of technologies for controlling post-translational modification processes in gene expression system

Masahiro Nagaya
(Material Chemistry, Material Science)

Keywords: *N*-glycosylation, Baculovirus expression system, *Antheraea pernyi*, lectin blot, 2D-sugar mapping, posttranslational modification

1. Introduction

Almost all the secreted and membrane-associated proteins of eukaryotic cells are glycosylated. Indeed, protein glycosylation, especially *N*-glycosylation, is more abundant than all other types of posttranslational modifications combined. *N*-linked glycoproteins are completed in the endoplasmic reticulum and further processed in the Golgi apparatus. The resulting oligosaccharides are classified into three groups: (1) high-mannose oligosaccharides, (2) complex oligosaccharides, and (3) hybrid oligosaccharides. These glycoforms are very important, because many studies have been revealing that glycan moieties of the glycoproteins have important roles in various biological events such as cell adhesion, cell differentiation and proliferation, immune response, neural functions, protein quality control, and so on.

Generally, baculovirus expression vector (BEV) systems possess protein-processing capabilities of insect cells, which can perform some mammalian-like posttranslational modifications, including glycosylation, and usually show productivity much higher than mammalian expression systems. Therefore, BEV systems have been frequently used for production of recombinant mammalian glycoproteins. In general, mammalian cells add complex type *N*-glycans often possessing terminal sialic acids, while insect cells add high mannose type or fucosylated paucimannose type *N*-glycans. Although variety has been found according to derived insect cell or produced glycoprotein, the difference in the glycoform between mammalian and insect cells indicates that the BEV systems has limitations of glycosylation for the production of mammlian-type modified glycoproteins.

Therefore, we attempted to develop a novel technique for controlling posttranslational *N*-glycosylation processes in the gene expression systems in insect cells such as AnPe cells. We studied the structures of *N*-linked oligosaccharide added on PTTH in several lepidopteran insect cell lines such as *Bombyx mori* (BmN4), *Spodoptera frugiperda* (Sf9), *Trichoplusia ni* (High5), *Spilosoma imparilis* (SpIm) and *Antheraea pernyi* (AnPe) using lectin blot analysis, identified the structures of *N*-glycans produced in Sf9 and AnPe using 2D sugar-mapping technique, and evaluated the potential abilities of the *N*-glycosylation pathway of AnPe cells to apply for the mammalian-type posttranslational *N*-glycosylation process.

2. The structural investigation of *N*-glycan produced in five lepidopteran insect cell lines using lectin blot analysis

Recombinant PTTH produced and secreted by each cell line showed the significant variation in apparent molecular mass ranging between 13 and 20 kDa. Differences in *N*-glycan structure and/or proteolytic processing were considered as major reasons. In fact, lectin blot analysis revealed that lectins GNA and AAA, which are specific to terminal α-linked mannose and α1,6-linked fucose respectively, clearly bound to recombinant PTTH produced by each cell line, while lectins RCA120, MAA and SNA, which are specific to β1,4-linked galactose, α2,3-linked sialic acid and α2,6-linked sialic acid respectively, did not bind to each PTTH sample. The results indicated that the majority of recombinant PTTH produced by AnPe as well as other lepidopteran cell lines carried fucosylated paucimannosidic *N*-glycans as generally observed in recombinant glycoproteins produced by BEV systems. In this study, all the results did not support the preliminary result indicating that AnPe added complex type *N*-glycans to the recombinant glycoprotein. However, it may be probable that amounts of complex type *N*-glycan added on PTTH were below detectable limits of lectin blot analysis. In addition, there is a possibility that PTTHs with sialylated *N*-glycan were removed during the preparation of crude PTTH samples by ion exchange

column chromatography, which was used for separation of charged *N*-glycans containing sialic acid from uncharged *N*-glycans. Therefore, we cannot conclude the inability of AnPe as well as other cell lines to form complex type *N*-glycan. Further analysis of *N*-glycan structure on affinity-purified recombinant PTTH in conjunction with biochemical and molecular biological analyses of the cell lines to identify glycosyltransferases and the responsible genes required for complex type *N*-glycan formation will provide us reliable answers.

3. The characterization and determination of *N*-glycans derived from baculovirus-infected AnPe and Sf9 insect cell lines using 2D sugar- mapping technique

To evaluate the *N*-glycosylation property of an insect cell line, *Antheraea pernyi* (AnPe), and used in a newly developed baculovirus expression vector system, *N*-glycans of purified PTTH produced by AnPe cells infected with a recombinant *A. pernyi* nucleopolyhedrovirus (AnpeNPV), were digested with glycoamidase A (from sweet almond), reductively aminated with 2-aminopyridine, and identified by two-dimensional high performance liquid chromatography (2D-HPLC) mapping technique. For comparison, *N*-glycans of PTTH produced by *Spodoptera frugiperda* cells (Sf9) infected with a recombinant *Autographa californica* NPV (AcNPV) were also analyzed similarly. Consequently, similarities and differences in the *N*-glycan structure composition between AnPe and Sf9 were revealed. *N*-glycans from AnPe contained 41.8% high mannose type, 32.8% paucimannosidic type, 12.5% monoantennary type, and 1.3% biantennary, complex type with terminal *N*-acetylglucosamine (GlcNAc) residues (Fig. 1a), while those from Sf9 contained 46.5% high mannose type, 29.8% paucimannosidic type, 7.7% monoantennary type, and no detectable biantennary complex type. In addition, one of the monoantennry type *N*-glycans with a terminal GlcNAc residue identified in AnPe was not detected in Sf9 (Fig. 1b). The proportion of *N*-glycans with an α-1,6-linked fucose residue at the innermost core GlcNAc residue was 41.4% in AnPe and 23.4% in Sf9, respectively. In both cell lines, mammalian-like complex *N*-glycans with terminal galactose and/or sialic acid residues were not identified. These results indicated that a reaction catalyzed by GlcNAc transferase II (GnTII), a key enzyme to form biantennary, complex *N*-glycans, occurs more efficiently in AnPe than in Sf9, suggesting that the proportion of complex *N*-glycans in AnPe cells may be largely enhanced by inhibiting the *N*-acetylglucosaminidase activity and/or supplying sufficient amounts of enzymes and substrates required for the sugar chain extension in the Golgi.

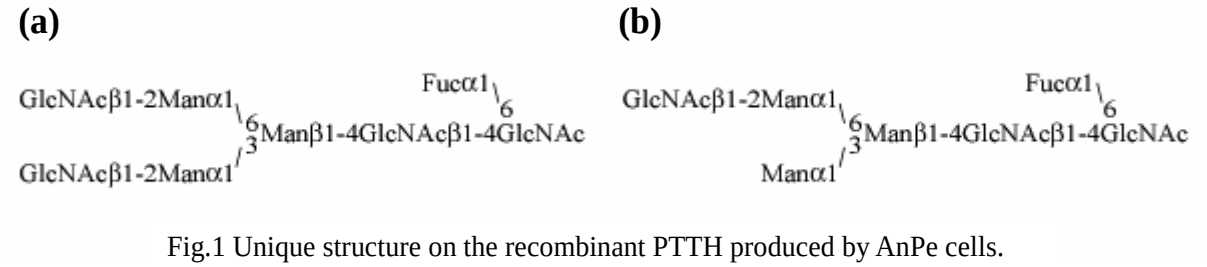

Fig.1 Unique structure on the recombinant PTTH produced by AnPe cells.

4. Conclusion remarks

Overall, the present study demonstrated that, although the AnPe cells possess typical *N*-glycosylation properties common in insect cells, they also possess an ability to add the complex *N*-linked oligosaccharides, but not the galacotose and sialic acid residues, suggesting that AnPe cells are suitable for production of mammalian-like glycoproteins, although the improvement to produce authentic glycoproteins is required. BEVsystem in AnPe cells must be widely used as a large-scale production system for therapeutic glycoproteins and as a system to elucidate a functional mechanism of oligosaccharide moieties of glycoproteins.

Author's publications

[1] Masahiro Nagaya, Jun Kobayashi and Tetsuro Yoshimura. Evaluation of N-glycosylation Property of Cultured Antheraea pernyi Cells in Comparison with Four Other Lepidopteran Cell Lines used in Baculovirus Vector S-ystems. Int.J. Wild Silkmoth & Silk. (2002) 7, 59-68.
[2] Masahiro Nagaya, Jun Kobayashi, Noriko Takahashi, Koichi Kato and Tetsuro Yoshimura. Two-dimensional High Performance Liquid Chromatography Mapping of Sugar Chains Demonstrated the Biantennary, Complex N-Glycan Addition to the Recombinant Glycoprotein Produced by Baculovirus-Infected Antheraea pernyi Ins-ect Cells. J. Insect Biotechnology & Sericology. (2003) 72, 79-86.